JOURNAL OF GEOPHYSICAL RESEARCH, VOL. 111, C08002, doi:10.1029/2005JC003254, 2006

Barotropic tides on the southeast New England shelf: A view from a hybrid data assimilative modeling approach

Ruoying He[1] and John L. Wilkin[2]

Received 28 August 2005; revised 21 April 2006; accepted 17 May 2006; published 1 August 2006.

[1] A high-resolution hybrid data assimilative (DA) modeling system is used to study barotropic tides and tidal dynamics on the southeast New England shelf. In situ observations include tidal harmonics of 5 major tidal constituents [M_2, S_2, N_2, O_1, and K_1] analyzed from coastal sea level and bottom pressure gauges. The DA system consists of both forward and inverse models. The former is the three-dimensional, finite difference, nonlinear Regional Ocean Modeling System (ROMS). The latter is a three-dimensional linearized, frequency domain, finite element model TRUXTON. The DA system assimilates in situ observations via the inversion for the barotropic tidal open boundary conditions (OBCs). Model skill is evaluated by comparing the misfits between the observed and modeled tidal harmonics. The assimilation scheme is found effective and efficient in correcting the tidal OBCs, which in turn improve ROMS tidal solutions. Up to 50% decreases of model/data misfits are achieved after inverse data assimilation. Co-amplitude and co-phase maps and tidal current ellipses for each of 5 tidal constituents are generated, revealing complex tidal variability in this transition region between the tidally amplified Gulf of Maine in the northeast and the tidally much less energetic Middle Atlantic Bight in the southwest. Detailed examinations on the residual circulation, energetics, and momentum balances of the M_2 tide reveal the key roles of the unique bottom bathymetry of Nantucket Shoals and the complex coastal geometry in affecting the regional tidal dynamics.

Citation: He, R., and J. L. Wilkin (2006), Barotropic tides on the southeast New England shelf: A view from a hybrid data assimilative modeling approach, *J. Geophys. Res.*, *111*, C08002, doi:10.1029/2005JC003254.

1. Introduction

[2] The continental shelf of southeastern New England south of Cape Cod, Massachusetts is located in the transition zone between the tidally amplified Gulf of Maine to the northeast and the tidally much less energetic Mid-Atlantic Bight shelf to the west (Figure 1). Because of its unique geographic location, complex coast/island geometry, and highly irregular bottom bathymetry of Nantucket Shoals, tides and tidal currents in this area are intrinsically complicated in their distributions and structures. Many physical and biogeochemical processes in the area are affected by the details of tidal dynamics. For instance, tides influence the extent of vertical mixing, and thus partially determine the location of temperature fronts that are often observable from satellite imagery (J. L. Wilkin, The summertime heat budget of the southeast New England shelf waters, submitted to *Journal of Physical Oceanography*, 2005) (hereinafter referred to as Wilkin, submitted manuscript, 2005). The strength of the tidal currents influences the bottom sediment distribution and short- and long-term fate of material and pollutants introduced into the water column. Similarly, both the vertical mixing and the tidal residual circulation affect the biological productivity by controlling the vertical distribution of nutrients and organisms and the advection of eggs and larvae.

[3] Albeit important, knowledge of tides and tidal dynamics in this area is still primitive, and largely based on a limited number of in situ point measurements [e.g., *Moody et al.*, 1984; *Brown*, 1984; *Limeburner and Beardsley*, 1982]. By combing recent field observations of currents and pressures with other historical data sets in the area into a large data assembly, *Shearman and Lentz* [2004] studied both barotropic and baroclinic tides, and provided valuable insights on tidal dynamics in a broader context of New England shelf waters. Revealing many complex features of the tidal dynamics, they concluded that under-sampling problems remain, and as such, a regional tidal modeling study is much needed to resolve and improve our understanding of tidal characteristics.

[4] Our objective is therefore to construct a high-resolution, regional tidal model to aid in dynamic interpolation and interpretation for this shelf region. The area of our interest is centered on Martha's Vineyard, and extends west-east from Narragansett Bay to the saddle of the Great South Channel, and north-south from Cape Cod out to just beyond the 60 m isobath at 40°30′N (Figure 1). As the first step, we

[1]Department of Applied Ocean Physics and Engineering, Woods Hole Oceanographic Institution, Woods Hole, Massachusetts, USA.
[2]Institute of Marine and Coastal Sciences, Rutgers, The State University of New Jersey, New Brunswick, New Jersey, USA.

0148-0227/06/2005JC003254$09.00

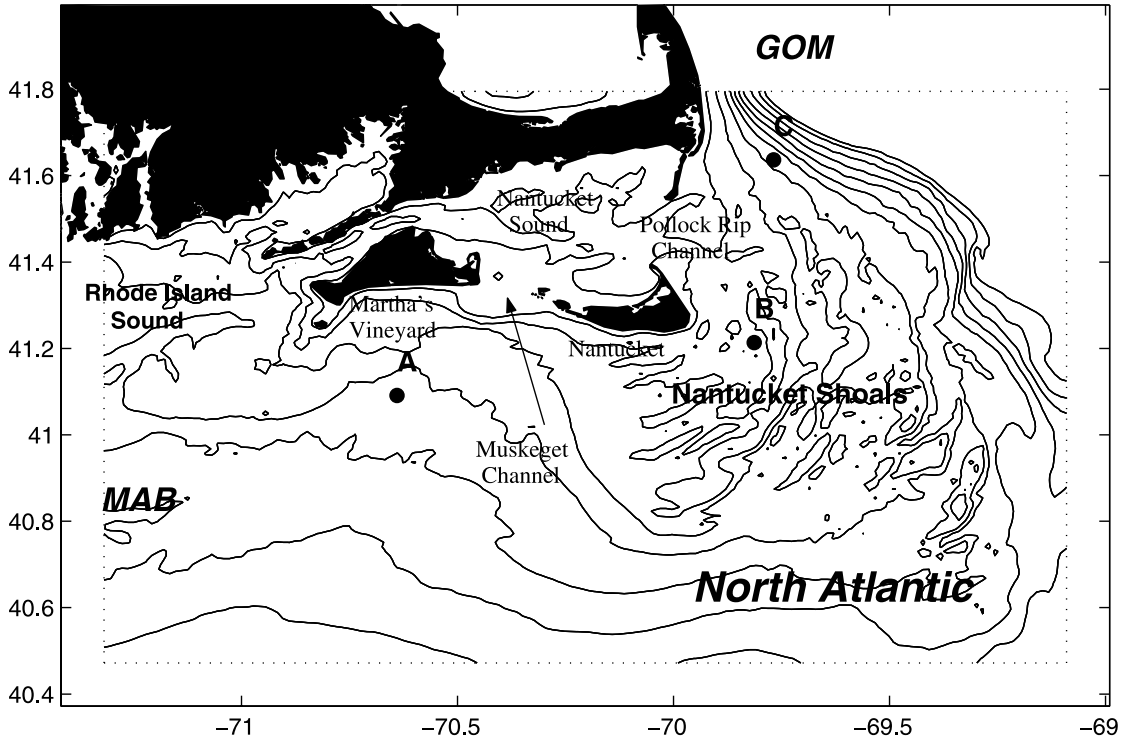

Figure 1. The region of research. Gray contours are the bottom bathymetry ranging from 10 m to 100 m. Dotted lines indicate the boundary of the regional tidal model. Stations A, B, and C are the locations where momentum balance analyses were performed (see details in section 5.4).

focus on modeling only the barotropic tides, which are highly energetic in this region. In limited area coastal domains the tides can be treated as being entirely remotely forced, i.e., the influence of the gravitational tide generating forces within the domain are negligible. The principal challenge to modeling tides accurately is the proper representation of tidal elevation and velocity boundary conditions around the entire model perimeter. The conventional way to achieve this is to use global/basin-scale tidal models to provide open boundary conditions (OBCs). Although significant progress has been made to improve global/basin-scale tidal models, and their solutions are fairly accurate in the open ocean and many shelf seas [e.g., *Shum et al.*, 1997], they are often not as accurate in coastal regions that have complex coastlines and bathymetric features (such as the New England shelf) due to limitations in their model resolutions and/or coarse resolution bathymetric data being used. This in turn impairs the global/basin-scale models' utility in providing OBCs for regional, high-resolution models. Often time, certain "fine tuning" of tidal OBCs is needed, and this is largely being done by trial-and-error based on empirical experience. *Lynch et al.* [2004] introduced an efficient inverse procedure to "fine tune" tidal OBCs for a regional South Atlantic Bight circulation model by inverse data assimilation. It is our goal here to construct a similar data assimilation modeling system to efficiently "fine tune" tidal OBCs by assimilating observed coastal tidal harmonics on the New England Shelf. The resulting "best estimations" of OBCs then drive our high-resolution regional model to produce best representation of and improved dynamic understanding on regional tidal circulation and dynamics.

[5] The remainder of this paper is organized as follows. Section 2 reviews in situ measurements that were used to derive tidal harmonics. The inverse data assimilation modeling system is presented in section 3. Inversion of tidal open boundary conditions and model validation are discussed in section 4. Co-amplitude and co-phase maps and tidal current ellipses are presented in section 5 to depict the tidal characteristics. Section 6 presents detailed examinations of the tidal dynamics, focusing on the strongest tidal constituent: the M_2 tide. Finally, section 7 summarizes and concludes the preceding material.

2. Observations

[6] In situ observations used in this study consist of 15 sets of tidal harmonic constants derived from an extensive collection of coastal sea level/pressure measurements distributed across the research domain. These include 9 sets of published tidal harmonics from the National Ocean Service [*NOS*, 2002] and U.S. Geological Survey (USGS) [*Moody et al.*, 1984], and 6 sets derived from bottom pressure measurements collected from the 1979–1980 Nantucket Shoals Flux Experiment (NSFE) [*Brown et al.*, 1985; *Beardsley et al.*, 1985], the Coastal Mixing and Optics (CMO) Experiment [*Dickey and Williams*, 2001], and Coupled Boundary Layers Air-Sea Transfer (CBLAST) experiment. For these bottom pressure time series, a standard harmonic analysis procedure [*Foreman*, 1977; *Pawalowicz et al.*, 2002] was used to generate tidal harmonics. Details of

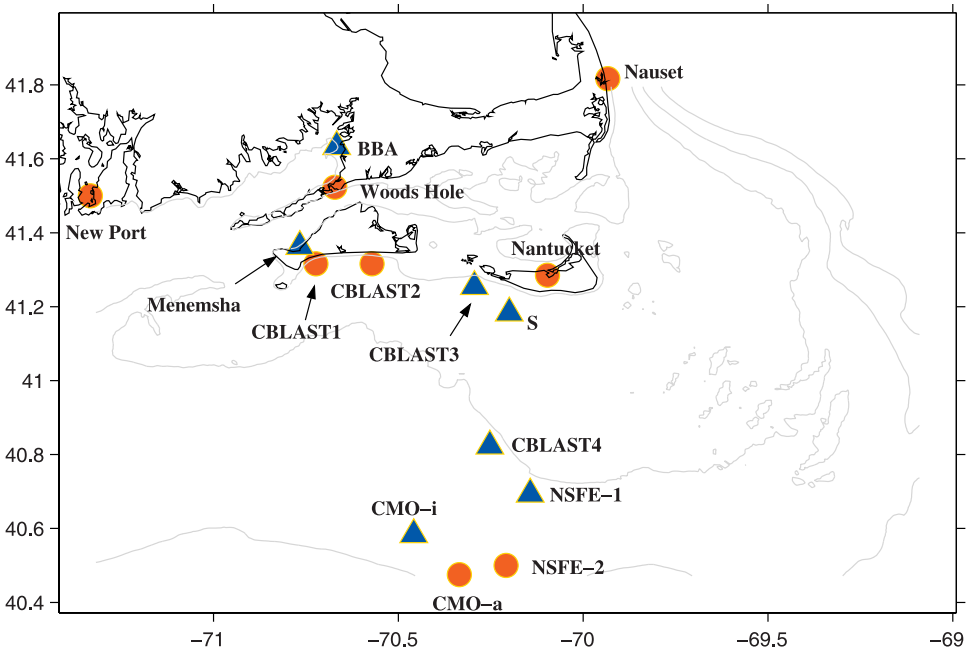

Figure 2. Locations of coastal tide gauges, and bottom pressure stations where harmonic constants (HC) of tidal elevations were derived. Dots indicate stations where HC were assimilated, and triangles denote stations where HC were used for model validation.

data processing were documented by *Shearman and Lentz* [2004]. Here, we focus on three major semidiurnal and two major diurnal tidal constituents, namely M_2, S_2, N_2, K_1 and O_1. Together, they account for 95% of total tidal variance on the New England Shelf.

[7] We purposely choose to use tidal harmonic constant observations from coastal tide gauge and bottom pressure observations because they are more accurate representations of barotropic tides than the current measurements, containing much less uncertainty introduced by small-scale bathymetric irregularity and oceanic processes. In particular, current measurements on the New England Shelf often contain signals of internal waves at tidal frequencies, as well as high-frequency internal solitons, and their magnitudes, phases and structures are highly variable, depending on forcing mechanism and the presence, strength, and structure of stratification [*Colosi et al.*, 2001; *Shearman and Lentz*, 2004].

[8] We divide these 15 stations into two groups. The first group includes stations (circles in Figure 2) close to either the land boundary or our tidal model's open boundaries. We refer to these as the "active" stations, which are used in data assimilation described below. The other group contains stations (triangles in Figure 1) largely distributed in the model interior. As such, we expect them to be good indicators to evaluate the model interior solution. These are used only as the validation set and are designated as "passive" stations.

3. Models and Hybrid Assimilation Scheme

[9] The data assimilation system consists of both forward and inverse components. The forward model is the three-dimensional, hydrostatic primitive-equation Regional Ocean Modeling System. It is a free-surface, finite-difference circulation model, formulated in a vertical terrain-following sigma-coordinate. The horizontal discretization is by an orthogonal curvilinear Arakawa-C grid. Our regional ROMS implementation for the New England Shelf has fine grid spacing (1 km) and realistic bathymetry from a 3-arc-second Coastal Relief Model [*Divins and Metzger*, 2003] augmented by soundings digitized from charts in the vicinity of Muskeget Channel (Figure 1). For the purpose of this study, the model density field is set to be homogenous. Open boundary conditions are specified following the method of *Marchesiello et al.* [2001] to apply Orlanski-type radiation to the three-dimensional velocity. The free surface (ζ) and depth-averaged velocity (u) boundary conditions use the radiation method of *Flather* [1976], i.e.,

$$u = u_t + \sqrt{g/h}(\varsigma - \varsigma_t)$$

where $\boldsymbol{g}$ is the acceleration due to the earth gravity, $\boldsymbol{h}$ is the local water depth, and $\boldsymbol{\zeta_t}$ and $\boldsymbol{u_t}$ are the estimations of tidal elevation and velocity boundary conditions to be specified, and thus the objects of our "fine tuning" approach.

[10] The inverse component of our system is the three-dimensional linearized, sigma-coordinate finite-element model TRUXTON [*Lynch et al.*, 1998]. Its discretization is harmonic in time, and finite element in space. TRUXTON was originally constructed as the inverse of QUODDY, a three-dimensional nonlinear finite-element forward circulation model [*Lynch and Naimie*, 1993]. The utility and effectiveness of TRUXTON in fitting QUODDY solutions to observations by deducing corrections to tidal OBCs has been demonstrated in modeling various coastal regimes with different circulation settings, such as the Gulf of Maine [*He et al.*, 2005], Georges Bank [*Lynch et al.*, 1998; *Aretxabaleta et al.*, 2005], and the South Atlantic Bight

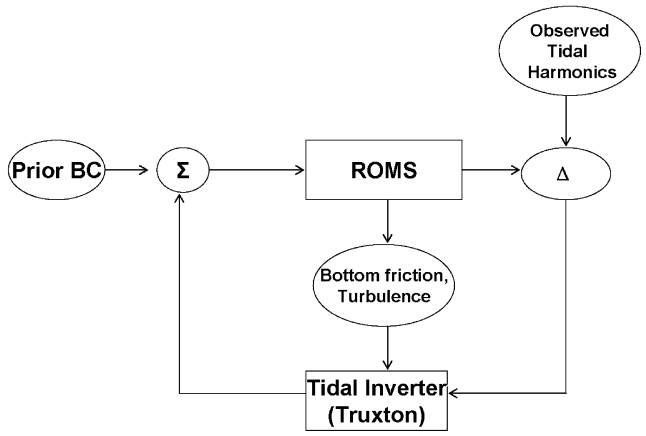

Figure 3. Flow chat of hybrid data assimilative tidal modeling system.

[*Lynch et al.*, 2004], to name a few. Mathematically, such inverse deduction is achieved by minimizing a quadratic cost function $\boldsymbol{J}$ in the least-square sense. Let $\boldsymbol{\eta}$ represent the unknown boundary elevation adjustment to be estimated and ε are the model/data misfits. The quadratic cost function $\boldsymbol{J}$ is defined as:

$$J = \frac{1}{N_\eta \sigma_\eta^2} \sum_{i=1}^{N_\eta} \varepsilon^2 + w_0 \oint \eta^2 ds + w_1 \oint \left(\frac{\partial \eta}{\partial s}\right)^2 ds$$

where σ_η is expected *error* of misfit ε, N_η is the numbers of observations, and *ds* denotes incremental distance along the model's open boundary. The first term on the right is the quadratic model/data misfit ε, which is defined as the complex difference between the observed and modeled tidal harmonics (i.e., tidal amplitude and phases in this case). The next two terms are the regularization terms, which penalize the size and spatial slope of boundary adjustment η to exert extra spatial constraint. $\boldsymbol{w_0}$ and $\boldsymbol{w}_1$ represent the inverse covariances of $\boldsymbol{\eta}$ and the elevation slope, respectively. For this New England Shelf application, we choose expected size of elevation misfit to be 0.05 m; expected size of boundary adjustment as 0.1 m; and expected slope of boundary adjustment as 10^{-7}. These three metrics were all weighted equally in the minimization, and their values are consistent with the order of magnitude of prior estimates of these quantities. Since misfit ε can be supplied from any forward model by comparing model solutions with observations, our premise is that by using TRUXTON and ROMS together, we can utilize interior observations to "fine-tune" ROMS tidal OBC. A hybrid data assimilation scheme such as this therefore provides a better alternative to the commonly used, empirical "trial-and-error" approach.

[11] The hybrid assimilation procedure (Figure 3) is as follows: (1) We start by running the ROMS forced by prior estimates of tidal open boundary conditions for a length of 30 days. This is based on *Emery and Thompson* [2001], who indicated that a record length of 30 days is sufficient to resolve the 5 major tidal constituents focused herein. Hourly ROMS simulated elevations are saved and analyzed by harmonic fitting to derive tidal harmonics for each of 5 tidal constituents; (2) The misfits between the observed and model tidal harmonics at "active" stations are used to drive the TRUXTON to deduce the correction to the tidal boundary conditions, and (3) the adjustments are added to the prior OBCs to form more accurate posterior open boundary elevation and velocity specifications, which subsequently drive another forward ROMS run.

[12] Although TRUXTON is a linear inverse model, it retains the principal nonlinearity of the tidal system (the motion-dependent frictions and vertical turbulence viscosity) by using the mixing and bottom stress coefficients generated by the forward model [*Lynch et al.*, 1998]. In our case, ROMS uses Mellor-Yamada turbulence closure, and the quadratic bottom stress law based on the near-bottom velocity u_b ($\tau = c_d|u_b|\vec{u}_b$, where C_d is the bottom drag coefficient, 0.003). As such, temporal means of both the pseudo drag coefficient $c'_d = c_d|u_b|$ and eddy viscosity N are passed on to TRUXTON during the inversion. An alternative way to specify the eddy viscosity used by TRUXTON is to follow *Lynch et al.* [2004] by defining $N = 0.2|ubar|^2$, where *ubar* is the ROMS depth averaged velocity. Sensitivity experiments show that for this barotropic tidal system, the inversion solutions are not sensitive to the way eddy viscosity is specified.

[13] The nonlinearity of the overall system requires that the process be iterated until no further improvement of the OBC (or equivalently, further improvement in forward model solutions) is achieved. Our results show that 2 iterations are sufficient, with the largest inverse deduction occurring after the first inverse iteration. It should be noted that because ROMS uses a structured (optionally curvilinear) rectangular grid, whereas TRUXTON use an unstructured triangle mesh, a prerequisite for using this hybrid data assimilative system is model gridding. To avoid potential inconsistency between the bathymetry and resolution of the two models, we purposely construct the unstructured mesh by directly subdividing the ROMS rectangle grid into triangles, thereby enhancing consistency of the two models. The TRXTON solutions at the unstructured nodes are them mapped to the ROMS boundary cells using nearest neighbor interpolation scheme with the assumption that with $\sim$500 m (the ROMS grid has 1-km spatial resolution), variations in tidal amplitude and phase are negligible.

4. Inverse Model Solutions and Validation

[14] Our "best" prior estimation of tidal OBCs was constructed with the tidal harmonics database from a two-dimensional, barotropic, boundary-fitting, finite-element Advanced Circulation (ADCIRC) model simulation of the western Atlantic [*Luettich et al.*, 1992; *CCAT Research Program*, 2003]. This product has been extensively used for tidal related purposes all along the U.S. East Coast [*Mukai et al.*, 2002].

[15] By assimilating tidal harmonics from "active stations", inverse deduction provides incremental fine tuning of amplitude and phase distributions for each constituent along the ROMS open boundary during each of two inverse iterations. These resulting data-inverted adjustments correct for the deficiency of "prior" OBCs, which as discussed earlier, largely come from the insufficiency of basin-scale model resolution and/or coarse resolution bathymetric data

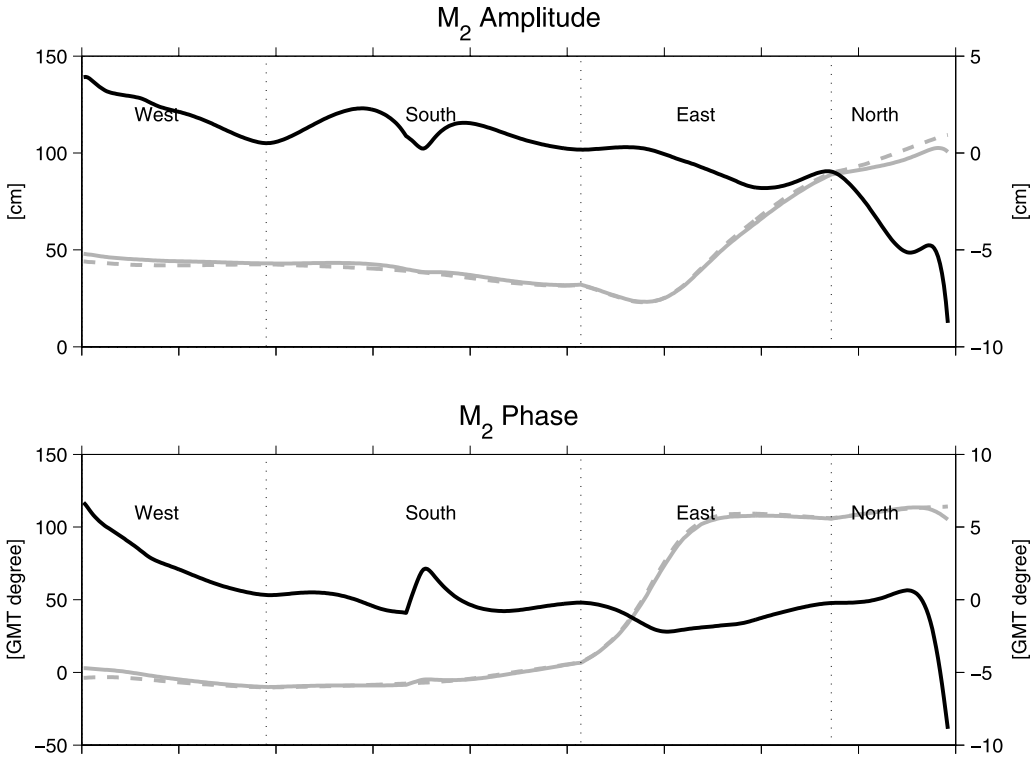

Figure 4. (top) Open boundary tidal amplitudes and (bottom) tidal phases for M_2 tide. The plots were drawn along the model's four open boundaries from the west, south, east to the north. In each panel, prior (dash gray), posterior (solid gray) are scaled by the y-axes on the left, while the refinements from data inversion (difference between posterior and prior, in solid dark) are scaled by the y-axes on the right.

being used. By looking at differences between the prior and the final posterior tidal sea level boundary conditions, we can see the impacts made by the inverse data assimilation. For the M_2 constituent (Figure 4), the adjustment in tidal amplitude is of order 5 cm or about 5–10% of the total tidal amplitude. The largest phase adjustments occur at the western (offshore of Narragansett Bay) and northern (the saddle of the Great South Channel) open boundaries, where

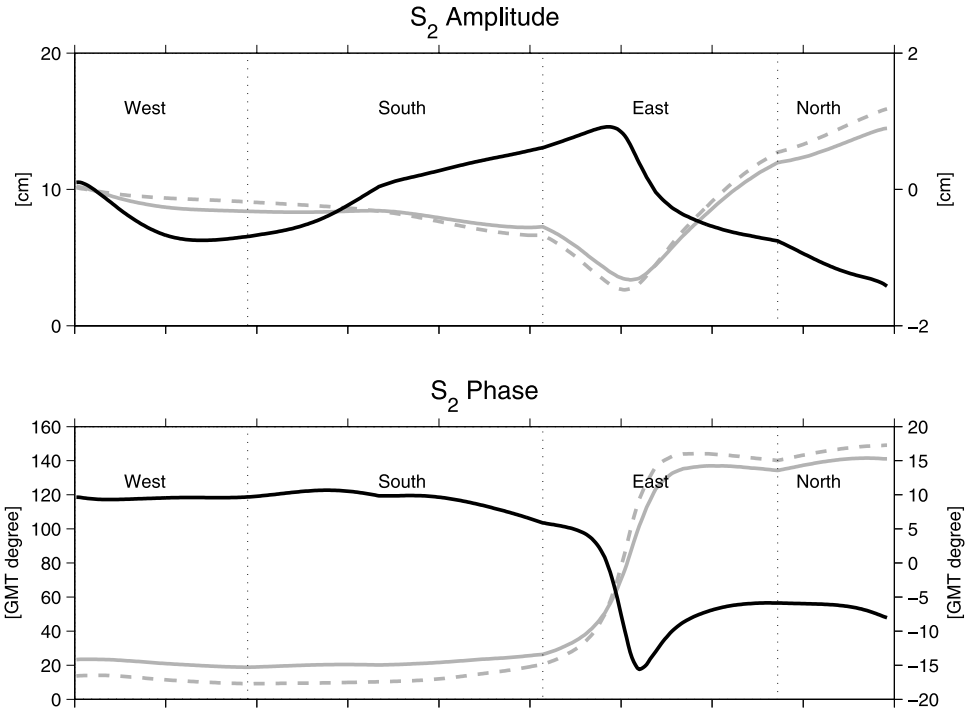

Figure 5. Same as Figure 4, but for S_2.

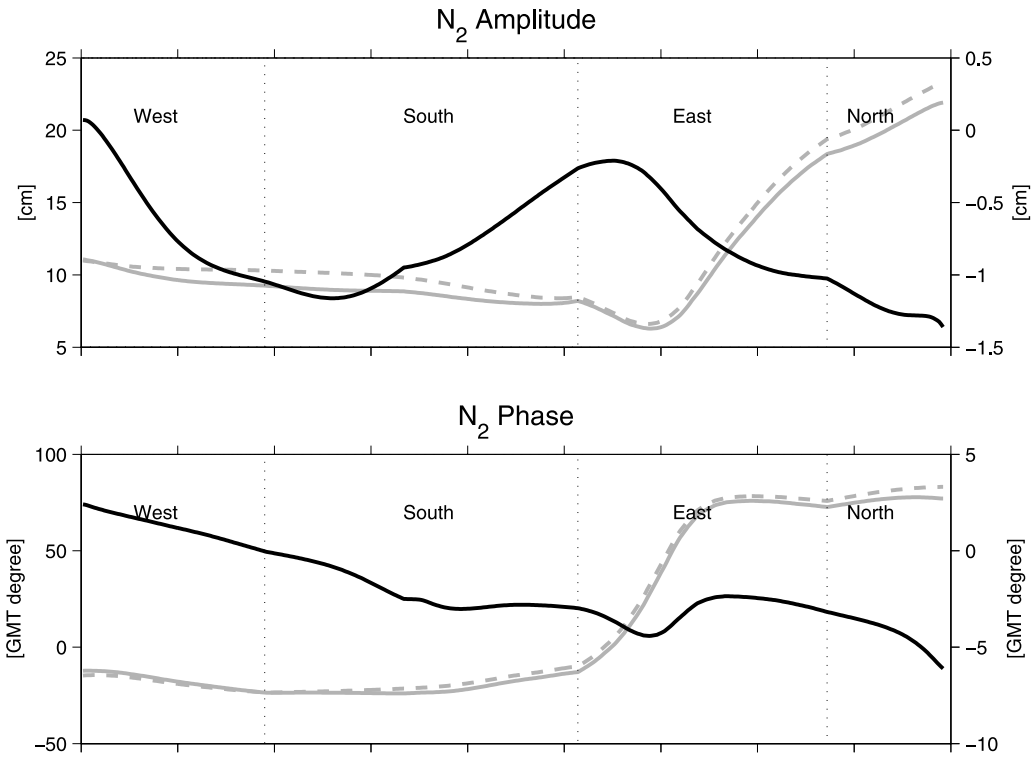

Figure 6. Same as Figure 4, but for N_2.

about 10° of change in the tidal phase is made. For S_2 (Figure 5), data inversion provides less than 2 cm adjustment in tidal amplitude (which is of order 10 cm), largely along the western and northern boundaries. The inversion increases tidal phase by up to 10° along the western and southern boundaries, while reducing the phases by 10° along a large portion of the eastern and the entire northern boundaries. Boundary adjustments for N_2 amplitude (which

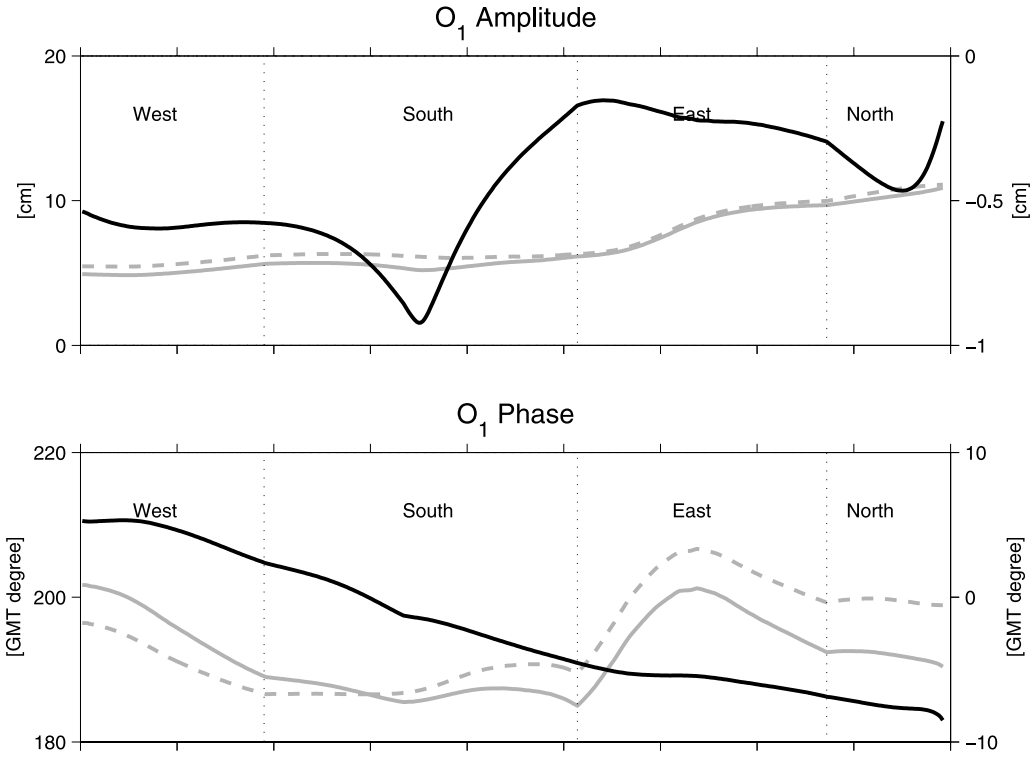

Figure 7. Same as Figure 4, but for O_1.

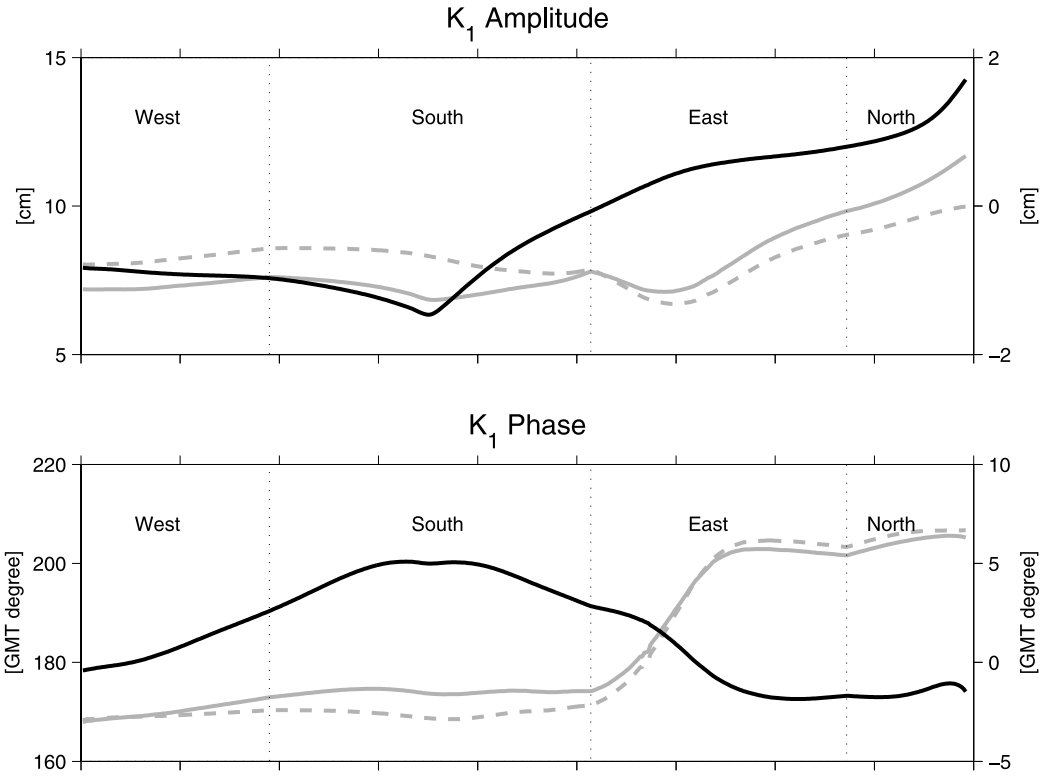

Figure 8. Same as Figure 4, but for K_1.

is of order 15 cm) are relatively subtle (Figure 6), with less than ±2 cm correction in amplitude. Corrections in tidal phase are less than 5°, and show a spatial pattern similar to that for S_2. Compared to semidiurnal constituents, diurnal tides (O_1 and K_1) along the open boundaries have smaller tidal amplitudes (of order 6 cm) and less spatial variability in tidal phases (Figures 7 and 8). Likewise, the corresponding adjustments from inverse deduction are less than 1.5 (2) cm in amplitude and less than 10° (6°) in phases for O_1 and K_1, respectively.

[16] Although these data-inverted adjustments seem small relative to the total tidal signals along the model's open boundaries, resolving and correcting for these errors are important as they tend to amplify as the tidal waves

Table 1. Harmonic Constants From Observation, ADCIRC, ROMS Prior, 1st Inversion, and Posterior by Stations for M_2 Tidal Constituent[a]

M2	Observations		ADCIRC		Prior		1st Inversion		Posterior		Model/Data Misfit (|Z − Zobs|)			
Stations	Amp	Phs	Amp	Phs	Amp	Phs	Amp	Phs	Amp	Phs	ADCIRC	Prior	1st Inv	Posterior
CBLAST1	40.70	349.88	37.06	351.34	37.60	348.87	40.60	349.66	41.60	350.21	3.77	3.10	0.20	1.00
CBLAST2	38.90	352.63	34.88	353.68	35.20	350.48	38.00	351.05	39.00	351.48	4.08	4.00	1.40	0.80
CMO_a	40.80	351.42	39.15	352.35	40.20	353.43	41.90	353.65	42.10	354.21	1.77	1.50	1.90	2.40
NSFE_2	38.20	358.48	38.13	353.23	39.40	353.79	40.90	354.12	41.20	354.72	3.5	3.40	4.10	4.00
WoodsHole	24.00	34.60	31.83	23.75	18.60	21.90	23.20	20.70	24.90	20.48	9.42	7.20	5.80	6.10
Nantucket	43.90	134.70	58.77	124.86	58.10	130.21	55.90	126.85	54.40	125.79	17.23	14.70	13.70	12.90
NEWPORT	51.30	1.00	43.49	355.74	44.80	355.95	49.90	359.67	51.10	1.37	8.93	7.70	1.80	0.40
NAUSET	103.20	102.00	109.47	114.16	110.60	114.88	103.20	110.94	100.90	107.98	23.38	25.10	16.10	10.90
Mean Misfits for Active Stations											**9.01**	**8.34**	**5.63**	**4.81**
CMO_i	41.10	352.00	39.36	352.95	40.00	353.34	41.70	353.37	42.10	353.67	1.86	1.50	1.20	1.60
CBLAST3	35.00	356.00	28.70	0.31	29.30	352.63	31.80	352.57	32.80	352.72	6.73	6.00	3.70	3.00
CBLAST4	38.20	354.75	36.55	358.26	35.50	358.11	37.40	357.88	38.00	357.99	2.82	3.40	2.20	2.20
NSFE_1	38.20	359.10	36.25	355.94	36.30	356.76	37.90	356.62	38.30	356.83	2.83	2.40	1.70	1.50
S	32.30	1.00	26.33	6.71	24.60	358.03	27.00	357.42	27.90	357.30	6.64	7.90	5.60	4.80
BBA	53.80	8.00	37.53	8.03	44.10	5.90	49.10	7.73	50.50	8.69	16.27	9.80	4.70	3.40
Menemsha	45.10	5.00	42.15	4.70	38.90	4.23	43.20	5.35	44.50	6.08	2.95	6.20	1.90	1.10
Mean Misfits for Passive Stations											**5.73**	**5.31**	**3.00**	**2.51**
Mean Misfits for All Stations											**7.48**	**6.93**	**4.40**	**3.74**

[a]Amplitude (amp) [cm], Phase (phs) [°], Misfit (|Z − Zobs|) [cm] are as defined in the text. Model outcomes and misfits are evaluated at the grid point nearest the data location. The top group lists the "active stations" in the inversion. The bottom group lists the "passive stations," which are used to verify the inversion. Also given are the mean misfits for both "active" and "passive" stations, along with the mean misfit for all stations.

Table 2. Same as Table 1, but for S_2 Tidal Constituent

S2	Observations		ADCIRC		Prior		1st Inversion		Posterior		Model/Data Misfit (|Z − Zobs|)			
Stations	Amp	Phs	Amp	Phs	Amp	Phs	Amp	Phs	Amp	Phs	ADCIRC	Prior	1st Inv	Posterior
CBLAST1	6.80	32.44	8.63	6.90	8.80	5.65	8.30	17.99	8.30	20.21	3.85	4.10	2.40	2.20
CBLAST2	6.50	34.09	8.18	7.81	8.30	6.12	8.00	18.96	8.00	21.30	3.71	4.00	2.40	2.20
CMO_a	9.10	17.21	8.40	10.28	8.50	11.41	8.50	21.00	8.50	22.27	1.27	1.00	0.80	1.00
NSFE_2	8.90	18.01	8.20	10.62	8.40	11.36	8.40	20.94	8.50	22.21	1.30	1.10	0.60	0.80
WoodsHole	6.10	35.60	7.37	25.58	5.70	15.27	5.80	33.23	6.10	34.88	1.73	2.10	0.40	0.10
Nantucket	4.70	166.70	6.52	155.89	6.50	163.98	6.80	149.30	6.60	144.58	2.10	1.80	2.70	2.90
NEWPORT	11.90	23.00	10.04	13.11	10.20	13.48	9.80	20.54	10.10	20.53	2.65	2.50	2.10	1.90
NAUSET	14.40	133.00	15.92	149.17	16.10	149.99	14.70	142.69	14.10	139.76	4.52	4.80	2.50	1.70
Mean Misfits for Active Stations											**2.64**	**2.67**	**1.74**	**1.60**
CMO_i	9.20	17.15	8.48	10.42	8.60	10.86	8.40	21.04	8.40	22.80	1.26	1.20	1.00	1.20
CBLAST3	6.00	36.03	6.86	9.48	7.20	5.93	7.10	20.06	7.20	22.52	3.07	3.60	2.20	2.00
CBLAST4	6.30	36.78	7.93	12.64	7.80	12.30	7.90	23.51	7.90	25.38	3.37	3.40	2.30	2.10
NSFE_1	8.80	22.22	7.85	11.46	7.90	12.05	8.00	22.62	8.10	24.32	1.83	1.70	0.80	0.80
S	7.80	21.00	6.21	12.30	6.30	7.25	6.40	22.22	6.60	24.61	1.91	2.20	1.40	1.30
BBA	11.60	32.00	9.10	17.85	10.50	19.27	10.20	29.69	10.30	30.67	3.56	2.70	1.50	1.30
Menemsha	10.00	24.00	9.44	17.46	9.00	15.85	8.70	26.67	8.80	27.74	1.24	1.70	1.30	1.30
Mean Misfits for Passive Stations											**2.32**	**2.36**	**1.50**	**1.43**
Mean Misfits for All Stations											**2.49**	**2.53**	**1.63**	**1.52**

approach inshore. Moreover, these adjustments all together are significant relative to the subtidal (e.g., wind-driven) signal, which is of order of 10 cm. This unfavorable signal-to-tide ratio makes it easy to smear the subtidal variability unless the tides are very precise. Hence, describing and understanding subtidal signals themselves call for the need for inverse deduction in the tidal bands.

[17] To see how the inverse deduction helps to improve ROMS fitting, we list both observed and modeled (prior, after 1st inversion, and posterior) tidal amplitude A and tidal phase Φ [GMT] at each station for each constituent in Tables 1–5. For side-by-side comparisons, tidal amplitude and phase are also transformed into complex tidal amplitude $Z = Ae^{-i(\pi/180)\phi}$, so that the model-data misfit is quantified as the complex difference between observed (Z_o) and ROMS modeled (Z_m) [*Lynch et al.*, 2004; *Davies et al.*, 1997]. Both "active" and "passive" stations are included in such comparisons to provide unbiased evaluation of the performance of the inversion. The mean complex misfits for prior, 1st inversion, and the posterior are calculated for each tidal constituent to assess the overall effectiveness of data inversion.

[18] It is found that ROMS prior solutions are better than or equivalent to ADCIRC solution. By successive inverse iteration, improvement is achieved for ROMS posterior/data comparisons for all 5 tidal constituents. As such, with respect to ADCIRC, 50%, 39%, 18%, 49% and 14% reductions in model-data mean misfit are obtained for M_2, S_2, N_2, K_1 and O_1, respectively. Note that because M_2 is one order of magnitude stronger than other tidal constituents, the fact that the most significant misfit reduction occur for M_2 implies that the inversion is successful. The model-data mean misfit of M_2 tide becomes smaller than the expected size of elevation misfit (5 cm) after only two inverse iterations, suggesting inverse deduction is efficient. For M_2, model-data misfits on each of both "active" and

Table 3. Same as Table 1, but for N_2 Tidal Constituent

N2	Observations		ADCIRC		Prior		1st Inversion		Posterior		Model/Data Misfit (|Z − Zobs|)			
Stations	Amp	Phs	Amp	Phs	Amp	Phs	Amp	Phs	Amp	Phs	ADCIRC	Prior	1st Inv	Posterior
CBLAST1	6.50	351.57	9.62	340.37	9.70	338.84	9.10	337.54	8.90	338.25	3.48	3.70	3.20	3.00
CBLAST2	6.40	353.42	9.24	342.70	9.30	340.75	8.70	339.54	8.50	340.15	3.18	3.40	2.90	2.70
CMO_a	9.70	334.19	9.81	338.53	10.10	339.11	9.00	336.80	8.70	335.76	0.75	0.90	0.80	1.00
NSFE_2	9.30	343.15	9.64	339.32	9.90	339.33	9.00	336.88	8.70	335.74	0.72	0.90	1.10	1.30
WoodsHole	8.00	19.40	9.65	9.73	7.00	14.45	7.00	14.06	7.20	14.52	2.22	1.20	1.20	1.00
Nantucket	11.30	102.50	13.94	88.60	13.70	94.10	13.30	90.18	13.10	88.64	4.03	3.00	3.30	3.40
NEWPORT	12.40	345.00	10.91	345.00	11.20	344.71	11.10	344.48	11.20	345.36	1.49	1.20	1.30	1.20
NAUSET	22.20	70.00	23.30	83.20	23.50	83.95	22.10	78.37	21.70	75.72	5.34	5.70	3.20	2.20
Mean Misfits for Active Stations											**2.65**	**2.50**	**2.12**	**1.97**
CMO_i	9.80	334.83	9.90	339.38	10.10	339.57	9.10	337.91	8.70	337.54	0.79	0.90	0.90	1.20
CBLAST3	6.10	357.07	8.11	348.90	8.10	344.10	7.50	342.93	7.40	343.07	2.24	2.60	2.20	2.10
CBLAST4	6.30	353.14	9.57	344.41	9.50	344.81	8.70	343.28	8.50	342.99	3.48	3.40	2.70	2.50
NSFE_1	9.20	314.87	9.40	342.03	9.50	342.72	8.70	340.77	8.40	340.02	4.37	4.50	4.00	3.90
S	9.10	339.00	7.71	354.01	7.40	349.81	6.80	348.75	6.80	348.59	2.59	2.30	2.60	2.70
BBA	13.80	351.00	10.46	357.34	12.00	354.65	11.70	354.34	11.70	355.38	3.6	2.00	2.20	2.30
Menemsha	11.90	356.00	11.24	351.76	10.70	352.09	10.30	351.51	10.30	352.45	1.08	1.40	1.80	1.70
Mean Misfits for Passive Stations											**2.59**	**2.44**	**2.34**	**2.34**
Mean Misfits for All Stations											**2.62**	**2.47**	**2.23**	**2.15**

Table 4. Same as Table 1, but for K_1 Tidal Constituent

K1	Observations		ADCIRC		Prior		1st Inversion		Posterior		Model/Data Misfit (|Z − Zobs|)			
Stations	Amp	Phs	Amp	Phs	Amp	Phs	Amp	Phs	Amp	Phs	ADCIRC	Prior	1st Inv	Posterior
CBLAST1	6.20	171.66	7.06	163.87	6.60	156.99	5.20	171.73	5.40	178.15	1.24	1.70	1.00	1.10
CBLAST2	6.40	173.87	7.05	165.43	6.50	158.97	5.20	173.68	5.50	179.33	1.18	1.70	1.20	1.10
CMO_a	7.30	173.72	8.40	169.04	8.40	168.40	7.00	174.04	6.80	175.84	1.27	1.30	0.30	0.60
NSFE_2	3.40	164.04	8.25	168.34	8.20	167.43	6.90	173.44	6.70	175.00	4.87	4.80	3.60	3.40
WoodsHole	7.10	189.00	8.26	173.95	8.20	168.14	6.80	178.32	6.80	184.25	2.32	3.00	1.30	0.60
Nantucket	9.20	221.60	8.62	201.69	8.40	203.43	8.80	208.48	9.10	209.23	3.13	2.90	2.10	2.00
NEWPORT	6.20	168.00	8.54	165.82	8.90	160.39	6.30	158.79	5.60	164.50	2.36	2.80	1.00	0.70
NAUSET	13.10	201.00	9.98	206.67	9.90	207.00	11.40	205.65	12.00	204.65	3.32	3.40	2.00	1.40
Mean Misfits for Active Stations											**2.46**	**2.70**	**1.56**	**1.36**
CMO_i	7.10	173.21	8.3	167.62	7.00	173.04	6.80	175.17	1.40	0.10	1.38	0.40	1.00	1.20
CBLAST3	6.30	178.31	6.1	164.38	5.40	179.44	5.70	183.15	1.50	0.90	1.1	0.80	2.20	2.00
CBLAST4	7.70	175.50	7.7	164.24	6.50	172.29	6.50	175.01	1.50	1.30	1.34	1.20	2.30	2.10
NSFE_1	6.40	173.89	7.7	164.54	6.50	172.29	6.50	174.43	1.70	0.20	1.7	0.10	0.80	0.80
S	6.10	177.00	6.2	166.47	5.60	180.36	5.90	183.44	1.10	0.60	1.02	0.70	1.40	1.30
BBA	6.60	168.00	8.6	162.15	6.40	167.12	6.10	173.49	2.10	0.20	1.69	0.80	1.50	1.30
Menemsha	5.40	176.00	8.3	160.02	6.20	165.95	6.00	172.19	3.40	1.30	3.17	0.70	1.30	1.30
Mean Misfits for Passive Stations											**1.63**	**1.81**	**0.66**	**0.67**
Mean Misfits for All Stations											**2.07**	**2.29**	**1.14**	**1.04**

"passive" stations are reduced from the prior to the posterior, indicating that we obtain a seamless domain-wide improvement of solution quality. The same conclusion is true for other major constituents. Admittedly, the boundary-fitting, finite-element ADCIRC model does quite decent job in simulating S_2, N_2, K_1 and O_1 tides.

5. Tidal Characteristics

[19] Given that ROMS, driven by refined OBCs, now provides tidal solutions that agree well with observations, we next use ROMS posterior solutions to produce the co-amplitude and co-phases charts for M_2, S_2, N_2, O_1 and K_1, and to further infer characteristics of the New England Shelf tides. It is seen that M_2 (Figure 9) tidal amplitude decreases from 0.4 m offshore of Martha's Vineyard to about 0.1 m over Nantucket Shoals, then rapidly increases to about 1 m toward the Gulf of Maine. This indicates the existence of a significant along-isobath pressure gradient, consistent with previous findings [*Brown*, 1984; *Shearman and Lentz*, 2004] that show the M_2 tide on the New England Shelf is more complicated than a simple standing or progressive plane wave. Similarly, M_2 tidal phase increases slightly from $-10°$ G to $0°$ south of Nantucket, then change dramatically to $100°$ G toward the model's northern boundary in the Great South Channel. Tidal amplitude and phases of S_2 and N_2 have very similar spatial patterns (Figures 10 and 11), although their amplitudes are much smaller, being only about 10–20% of M_2. For all three semidiurnal constituents, one unique common feature is a local amplitude minimum over Nantucket Shoals. This is the transition region between the dynamically distinct Mid-Atlantic Bight (MAB) shelf to the west and the semi- diurnally amplified Gulf of Maine (GOM) to the northeast. Co-phase charts

Table 5. Same as Table 1, but for O_1 Tidal Constituent

O1	Observations		ADCIRC		Prior		1st Inversion		Posterior		Model/Data Misfit (|Z − Zobs|)			
Stations	Amp	Phs	Amp	Phs	Amp	Phs	Amp	Phs	Amp	Phs	ADCIRC	Prior	1st Inv	Posterior
CBLAST1	5.20	199.64	5.17	200.86	4.50	205.27	4.80	205.80	5.00	205.71	0.11	0.80	0.70	0.60
CBLAST2	5.20	200.04	5.33	200.96	4.70	206.12	4.90	206.14	5.20	205.71	0.16	0.70	0.60	0.50
CMO_a	5.40	182.90	6.18	186.78	6.10	187.17	5.50	187.21	5.20	187.12	0.88	0.80	0.40	0.40
NSFE_2	2.40	189.39	6.05	187.50	6.00	187.72	5.30	187.19	5.10	186.60	3.65	3.60	2.90	2.70
WoodsHole	6.60	203.70	6.18	198.40	5.40	195.10	5.70	195.35	5.90	196.75	0.72	1.50	1.30	1.00
Nantucket	8.40	215.90	8.98	207.74	9.20	210.30	8.80	205.16	8.80	203.00	1.36	1.10	1.70	2.00
NEWPORT	4.90	199.00	5.17	193.13	4.60	187.70	4.60	198.59	4.80	204.47	0.58	1.00	0.30	0.50
NAUSET	11.50	182.00	11.10	198.88	11.00	199.52	10.70	191.80	10.70	188.38	3.34	3.50	2.10	1.40
Mean Misfits for Active Stations											**1.35**	**1.62**	**1.25**	**1.14**
CMO_i	5.20	184.17	6.06	187.62	6.00	187.78	5.40	188.53	5.30	188.93	0.92	0.90	0.50	0.40
CBLAST3	5.50	199.07	5.81	202.37	5.30	208.33	5.40	206.79	5.60	205.43	0.45	0.90	0.70	0.60
CBLAST4	5.60	189.48	5.58	191.21	5.40	192.33	5.10	192.90	5.10	192.88	0.17	0.30	0.60	0.60
NSFE_1	5.20	191.36	5.58	191.03	5.50	191.51	5.10	191.64	5.00	191.24	0.38	0.30	0.10	0.20
S	5.80	197.00	6.00	201.70	5.40	206.93	5.50	204.78	5.70	203.26	0.52	1.00	0.80	0.60
BBA	4.90	204.00	5.76	197.92	4.90	195.33	4.90	201.35	5.10	204.52	1.02	0.70	0.20	0.30
Menemsha	6.00	195.00	5.30	193.37	4.80	192.67	4.90	198.04	5.00	200.86	0.72	1.20	1.20	1.10
Mean Misfits for Passive Stations											**0.60**	**0.76**	**0.59**	**0.54**
Mean Misfits for All Stations											**1.00**	**1.22**	**0.94**	**0.86**

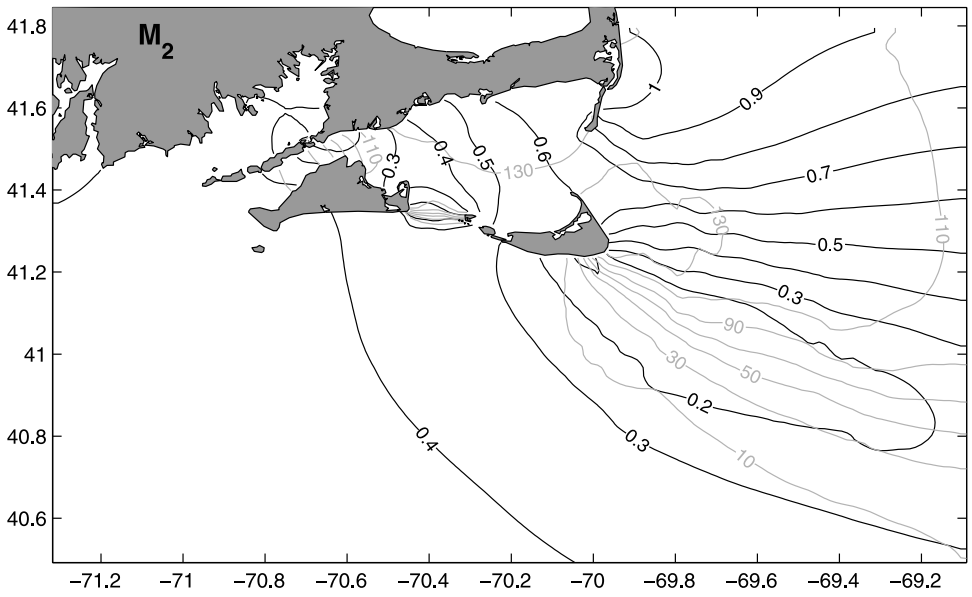

Figure 9. Modeled M2 tidal co-amplitude (in m, thick lines) and co-phases (degree, GMT; light lines).

show that there is about 90–120° elevation phase lag between the MAB and the GOM for all three semidiurnal tides. Kinematically, the semidiurnal tides of the two regions are out of phase and counteracting each other, resulting in relatively low tidal elevations in this transition zone.

[20] In contrast, diurnal constituents K_1 and O_1 show rather small amplitude and phase variations across the New England Shelf (Figures 12 and 13). Since these tides are not amplified, diurnal tides in GOM and MAB are quite similar and largely in phase. This is consistent with previous finding [i.e., *Daifuku and Beardsley*, 1983]. Both amplitude and phase slowly increase from the southwest to the northeast. Compared to M_2, the shelf-wide tidal amplitude of K_1 and O_1 are very small, being only ~10% of the counterpart of M_2.

[21] The character of the tide in a particular region can be generally described in terms of the amplitude ratio between diurnal and semidiurnal tidal constituents, i.e., $F = (K_1 + O_1)/(M_2 + N_2 + S_2)$. *Defant* [1958] provides the following interpretations:

$F = 0.0 - 0.25$, semidiurnal

$F = 0.25 - 1.50$, mixed, predominantly semidiurnal

$F = 1.50 - 3.0$, mixed, predominantly diurnal

$F > 3.0$, diurnal

Based on this, the tidal regime (Figure 14) on the southeast New England Shelf can be generally characterized as mixed and mainly semidiurnal type, although significant deceases in amplitudes of semidiurnal tides in the Nantucket Shoals

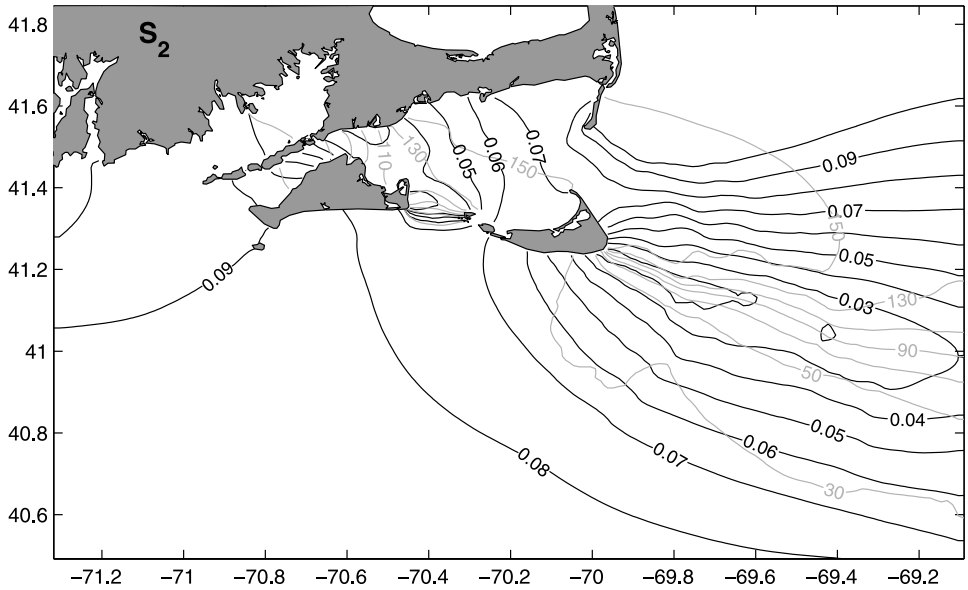

Figure 10. Same as Figure 9, but for S_2.

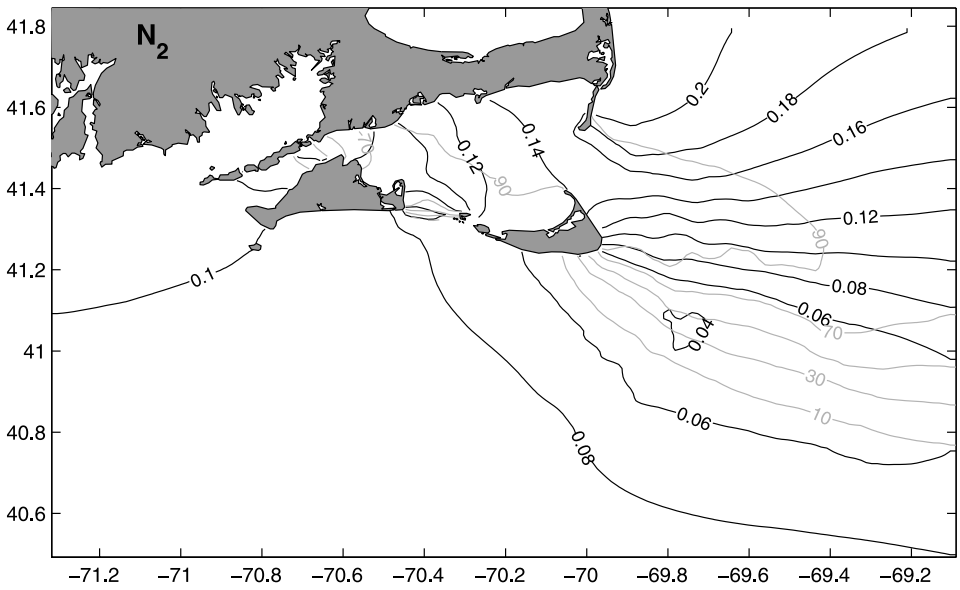

Figure 11. Same as Figure 9, but for N_2.

area make the role of diurnal tides more important, especially in the region very close to the coast.

[22] Using ROMS's posterior solutions, characteristics of tidal currents are depicted by the depth-average tidal current ellipses for each tidal constituent (Figures 15–19). The strongest M_2 tidal currents are found to be $\sim$1.5 ms^{-1}, located in Muskeget Channel and the southeast of Nantucket Island. The rapid decrease in tidal current speed seen west of Nantucket Shoals is thought to be responsible for the accumulation of fine-grained sediment on the mid-shelf between 70°W and 71.3°W [*Bothner et al.*, 1981; *Twichell et al.*, 1981]. The major axes of tidal current ellipses are approximately parallel to local isobaths, except in Muskeget Channel, where the major axis of the tidal current is perpendicular to the isobath. Tidal currents of S_2 and N_2 share the same spatial patterns of M_2, although the speeds are much weaker, with the largest being $\sim$0.25 ms^{-1} (note the change of velocity vector scale between M_2 and S_2/N_2). For diurnal constituents, tidal currents are even smaller and exhibit limited spatial variability. The largest current speed is about 0.1 ms^{-1}. As for the semidiurnal tide, the major axes of the diurnal tidal current ellipses are largely parallel to the local isobaths.

6. Tidal Dynamics and Tidal Residual Circulation

[23] Since the M_2 is by far the strongest tidal component in the system, we now focus on it alone to explore the

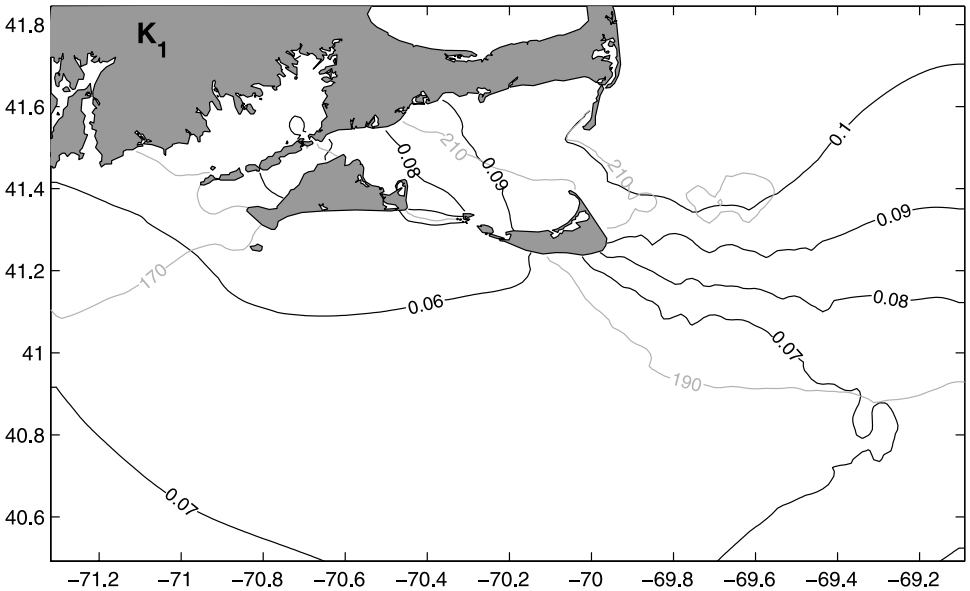

Figure 12. Same as Figure 9, but for K_1.

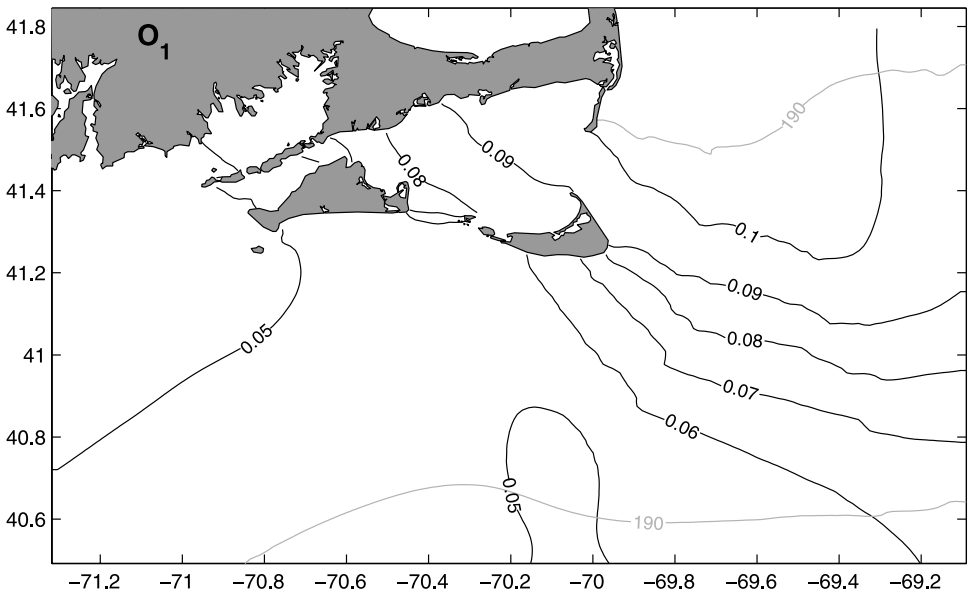

Figure 13. Same as Figure 9, but for O_1.

details of the tidal mixing, residual circulation, energy properties and momentum balances.

6.1. M_2 Tidal Mixing Parameter

[24] *Simpson and Hunter* [1974] examined the role of tidal turbulence in generating mixing fronts. A critical value of $\boldsymbol{U^3/H}$ was shown to be able to predict the location of mixing fronts in the shelf sea. Using the depth-averaged M_2 tidal velocity for $\boldsymbol{U}$, we can apply the ROMS posterior solution to determine the front location due to tidal mixing and $\mathbf{log_{10}}$ $(\boldsymbol{h/U^3})$ is shown in Figure 20. Here we see low values of $\boldsymbol{h/U^3}$ over Nantucket Shoals, the shallow region inside Nantucket Sound, and in Muskeget Channel. Thus we expect tidally induced vertical mixing to be a dominant dynamical player in these portions of the domain. The contribution of tidal mixing in the generation of property fronts is supported by satellite sea surface temperature images that often show waters that are relatively cooler than the surrounding shelf waters in this area (Wilkin, submitted manuscript, 2005). Because of the counteracting effects of tidal mixing and local stratification by surface and lateral buoyancy fluxes, the location and structure of fronts are highly variable. Previous study suggests that a critical value of $\mathbf{log_{10}}$ $(\boldsymbol{h/U^3})$ of 1.9 characterizes the range of location of tidal fronts [*Greenberg*, 1982]. Based on this, the

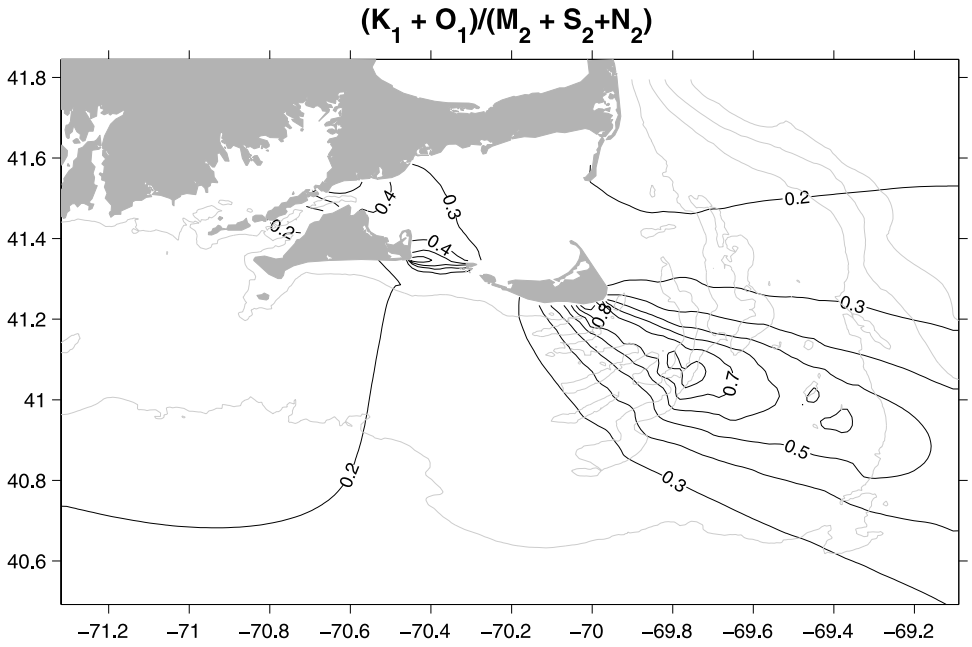

Figure 14. F-ratio for the study region.

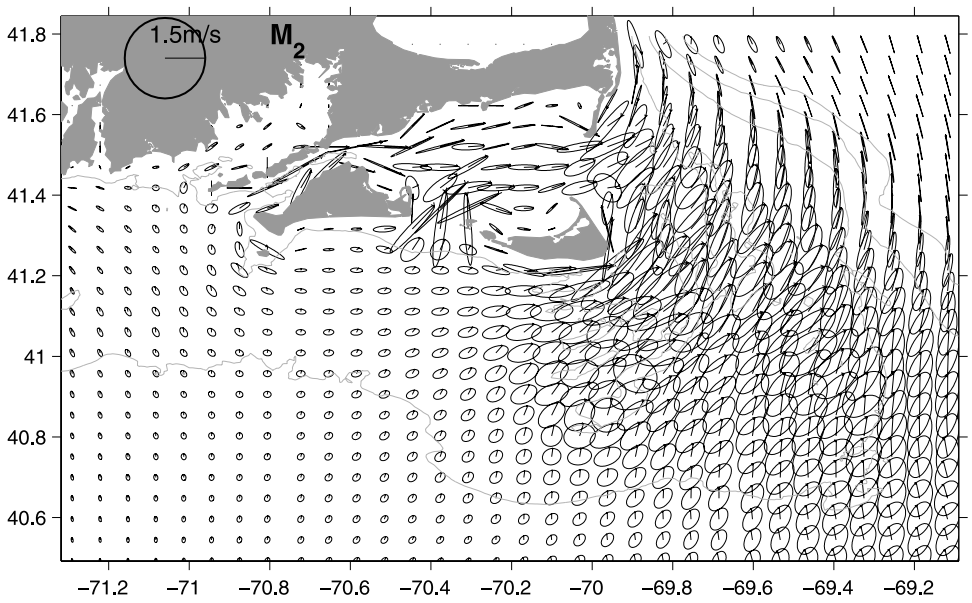

Figure 15. Depth-averaged tidal current ellipses for M_2. Tidal ellipses are plotted every 5 grid points.

location of the tidal mixing front southeast of Nantucket is expected to fall between 40 m to ~70 m isobaths.

6.2. M_2 Tidal Residual Circulation

[25] Due to variable bathymetry, the tidal flow may generate residual currents through nonlinear interaction [*Zimmerman*, 1978]. These tidal residual currents often play an important role in the local mean circulation and material property transport. To extract the time-averaged residual motion, the ROMS posterior M_2 tidal currents were averaged over a 12.42-hr period, and the result of this average is shown in Figure 21. The residual circulation is strong, with the maximum speed of 0.1 m s^{-1} (or approximately 10 km day^{-1}). One portion of the residual mean flow seems to enter the New England Shelf from the east. The other large portion of residual circulation enters the shelf from the Great South Channel. Once reaching east of Nantucket, the portion of circulation bifurcates, one branch moving eastward and the other moving south. The latter branch then joins the currents from the east; together they flow westward to the MAB. Such a spatial pattern may be generated by sharp changes in the coastline and rough bottom bathymetry. It implies unique and effective pathways for material property transport from the GOM to the MAB, and from the ocean interior to the shelf.

6.3. M_2 Tidal Energy and Dissipation

[26] Given that tidal currents on the New England shelf are strong, it is of interest to see the structure of the barotropic tidal energy flux [*Kowalik and Proshutinsky*,

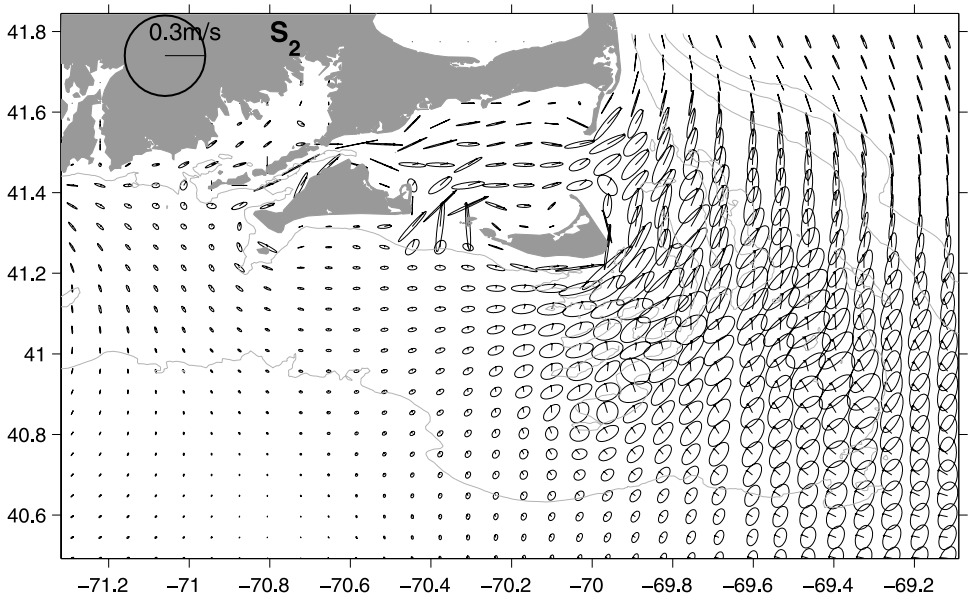

Figure 16. Depth-averaged tidal current ellipses for S_2. Tidal ellipses are plotted every 5 grid points.

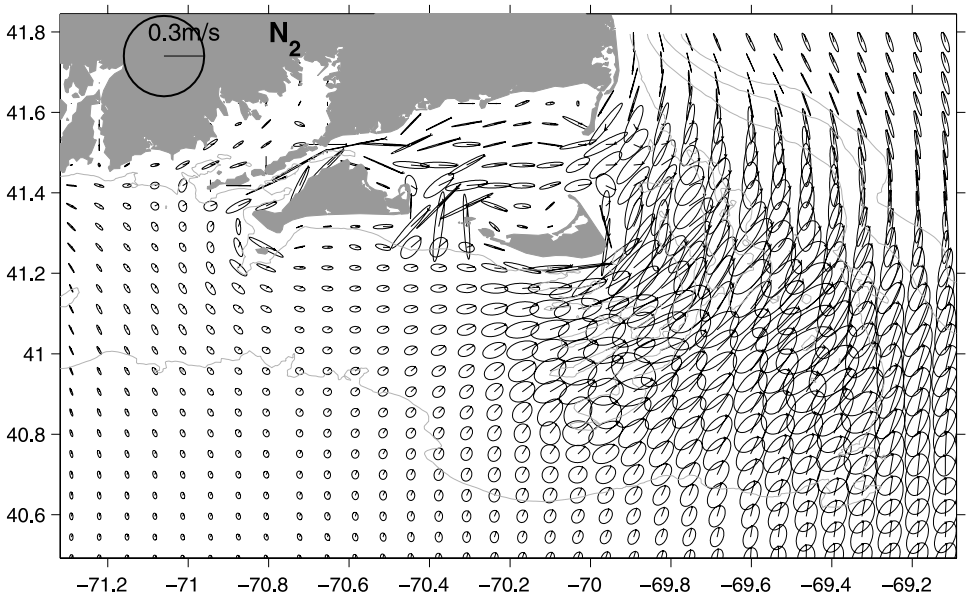

Figure 17. Depth-averaged tidal current ellipses for N_2. Tidal ellipses are plotted every 5 grid points.

1993] which, when including the contribution of both kinetic and potential energy, is given by:

$$\vec{F} = (h+\eta)\rho_0\left(0.5|\vec{u}|^2 + g\eta\right)\vec{u}$$

where h is the water depth, η is the tidal elevation, ρ_0 is the seawater density (1026 kg/m^3), $\vec{\boldsymbol{u}}$ is the ROMS posterior depth-averaged current velocity vector, and g is the acceleration due to gravity. The mean M_2 energy flux (Figure 22) was computed by averaging the flux time series obtained from the above equation over the M_2 tidal period. A striking feature revealed here is that tidal energy fluxes from the Gulf of Maine to the north and the Atlantic Ocean to the south converge on Nantucket Shoals. Part of this confluent energy flux moves eastward to the interior of the North Atlantic, and the rest appears to be dissipated locally. The Nantucket Shoals are therefore a significant tidal energy sink.

[27] To investigate further the dissipation of the M_2 tides quantitatively and identify areas with the highest tidal energy losses, we compute the rate of energy dissipation as defined by *Munk* [1997]:

$$D = \frac{1}{T}\int_0^T C_d\rho_0\left(u^2+v^2\right)^{3/2}dt$$

where C_d is the bottom drag coefficient (0.003), ρ_0 is the seawater density (1026 kg/m^3), u and v are the posterior M_2

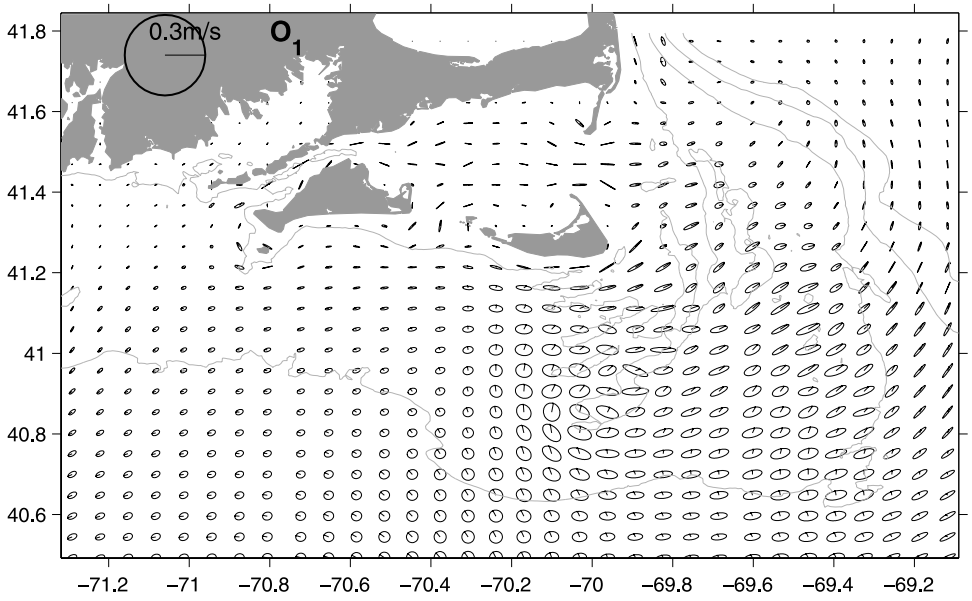

Figure 18. Depth-averaged tidal current ellipses for O_1. Tidal ellipses are plotted every 5 grid points.

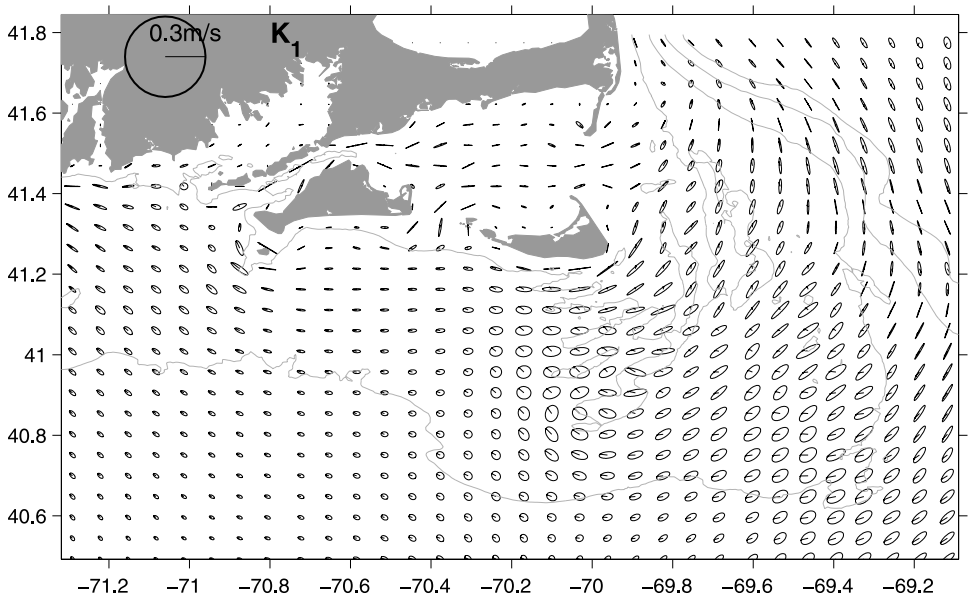

Figure 19. Depth-averaged tidal current ellipses for K_1. Tidal ellipses are plotted every 5 grid points.

depth-average tidal velocity components at each grid point, and T is the M_2 tidal period. The spatial distribution (Figure 23) of M_2 dissipation rate demonstrates that indeed Nantucket Shoals have the largest dissipation rate ($\sim$10 W/m^2). This is not unexpected, because both strong currents and rough and irregular bottom bathymetry on Nantucket Shoals can contribute to the high dissipation in this area. Two other regions with high dissipation rate are identified. One is located in Muskeget Channel region and the other in the waters between Woods Hole and Martha's Vineyard. Both places have strong tidal currents (Figure 15) due to the local geometric constrictions of the narrow water gateway. This highlights how coastal geometry impacts on the circulation structure and energy distribution.

6.4. M_2 Tides Momentum Balance

[28] *Shearman and Lentz* [2004] examined the momentum balance of M_2 tides in the depth-averaged

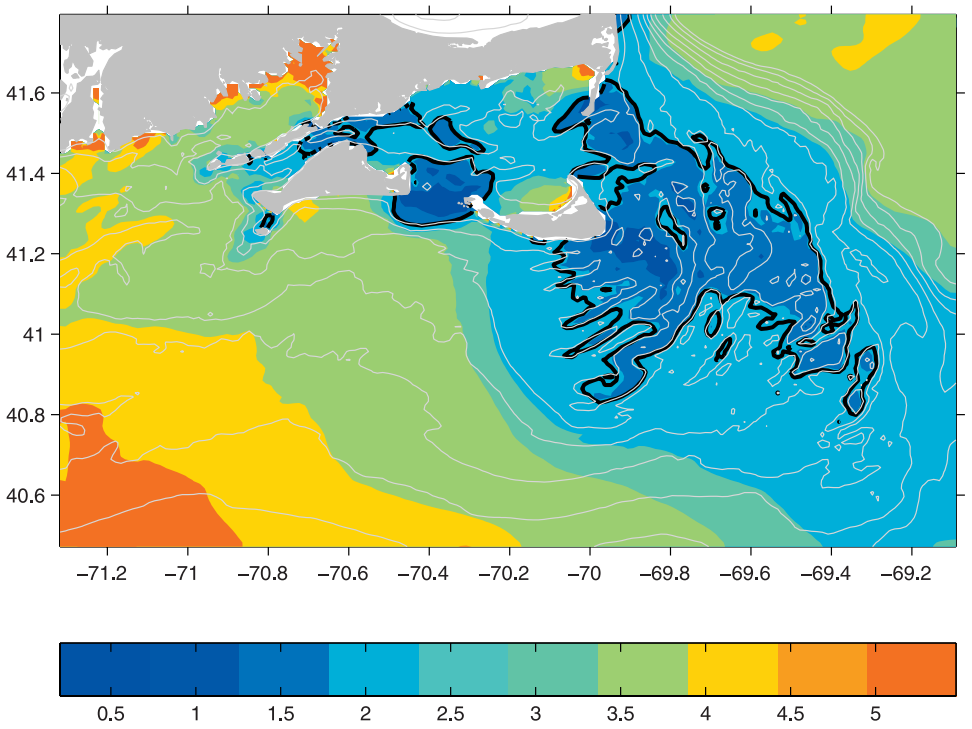

Figure 20. Tidal mixing parameter $\mathrm{Log}_{10}(h/U^3)$ for M_2 tidal currents. Solid, dark contour line indicates 1.9, defining the tidally induced frontal locations.

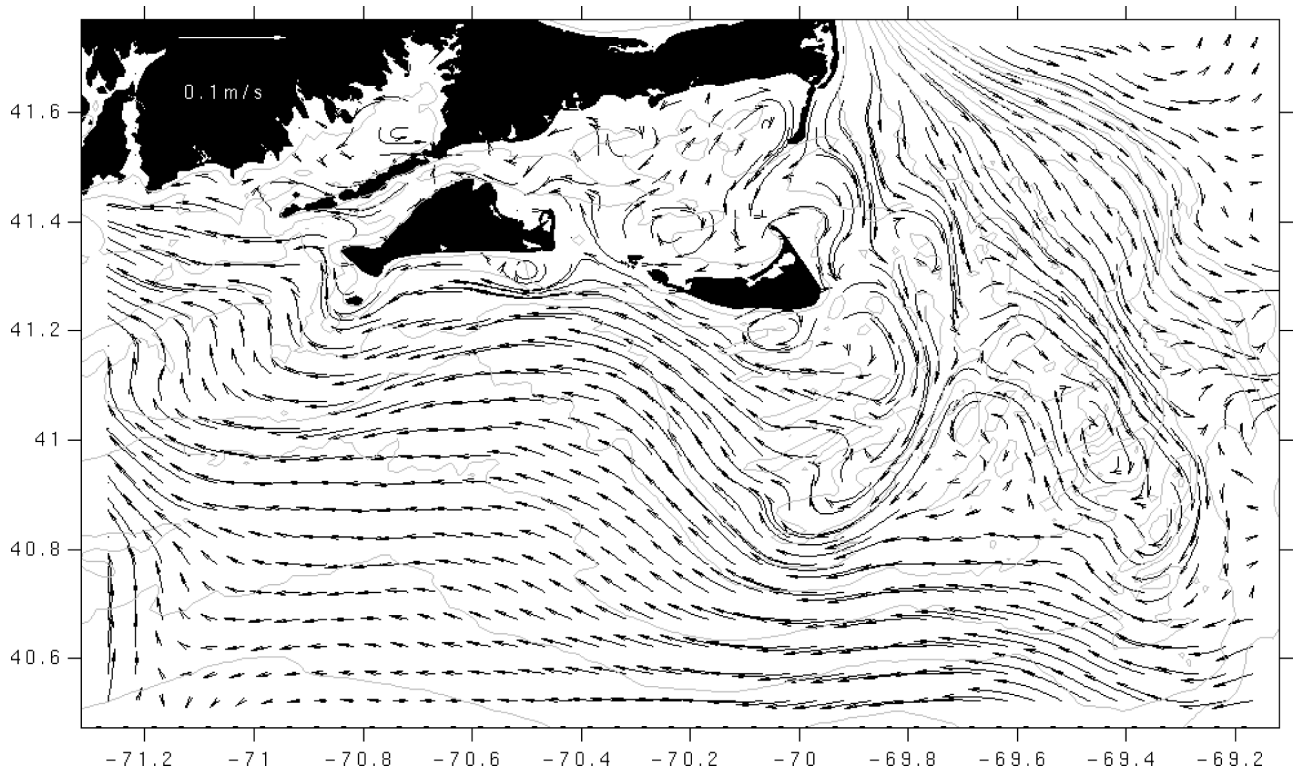

Figure 21. Depth-averaged M2 tidal residual circulation.

horizontal momentum equations based on in situ current and pressure observations south of Martha's Vineyard (CMO data set). They found the local acceleration term is the largest, followed by Coriolis and pressure gradient, and that the nonlinear term and bottom stress are more than an order of magnitude smaller. A similar distribution of momentum was also found by *Brown* [1984].

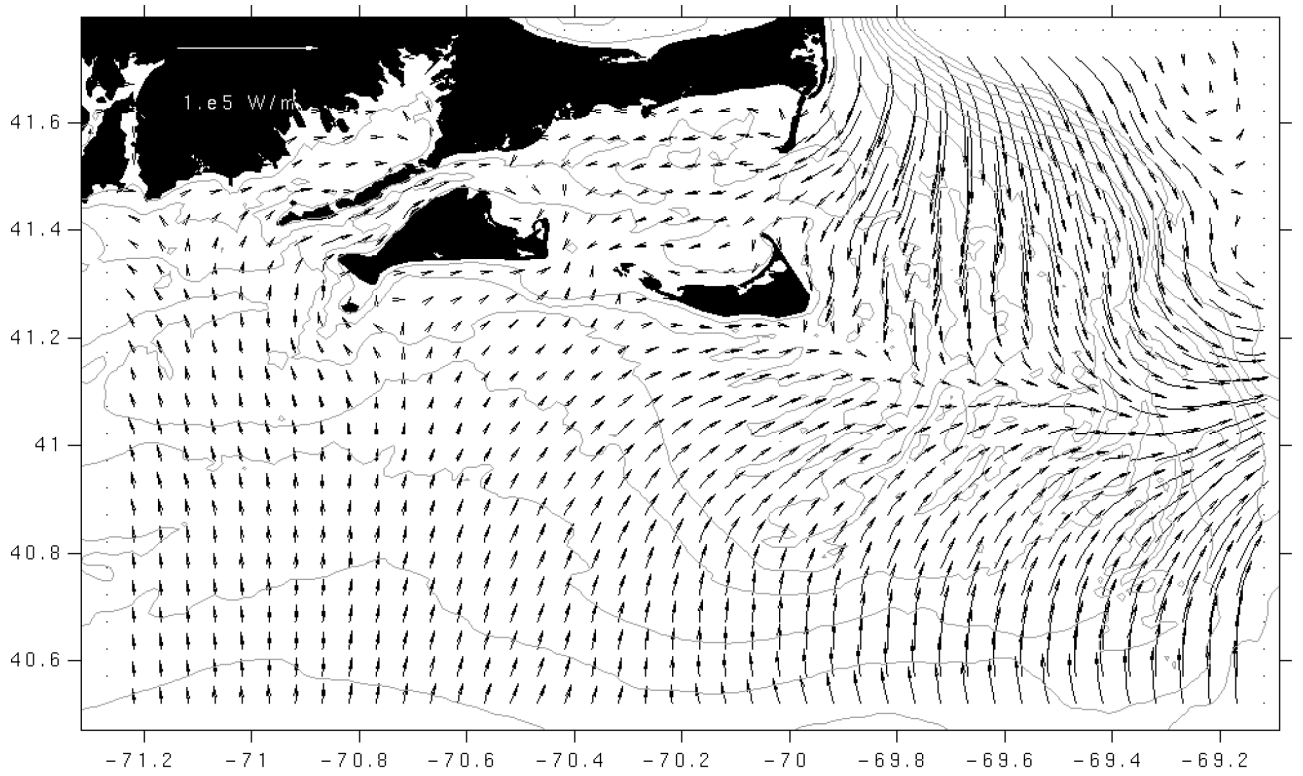

Figure 22. M_2 mean tidal energy flux per unit length (in W/m).

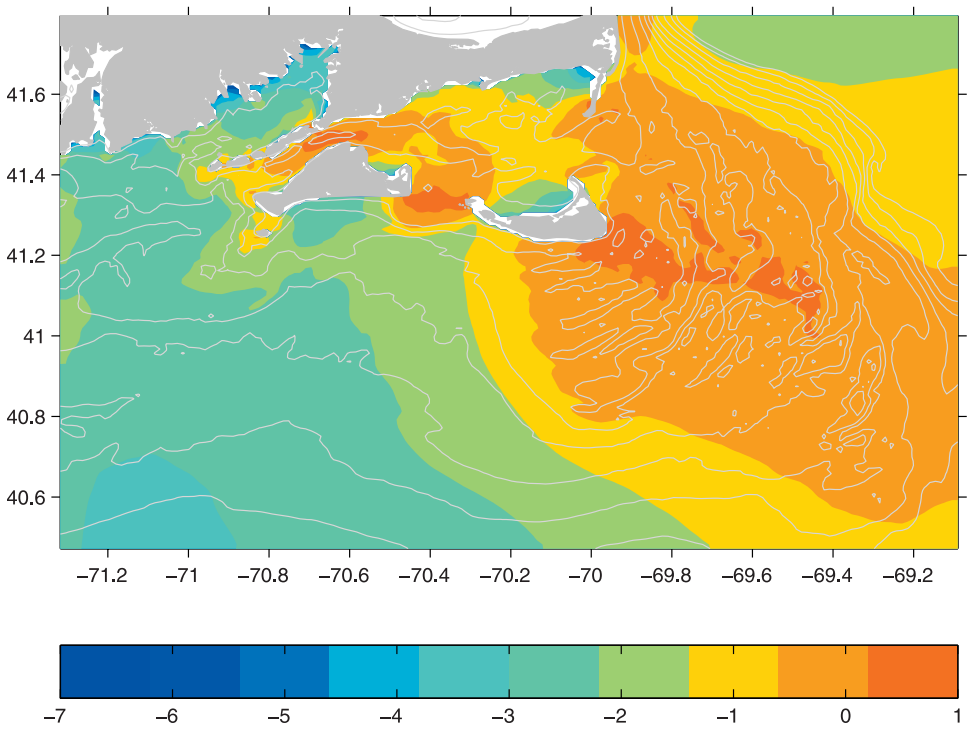

Figure 23. M_2 mean tidal energy dissipation rate (W/m^2). Values are scaled by $\log_{10}$.

[29] To compare with these observations, we use ROMS posterior solution to perform depth-averaged momentum balance analysis for M_2 tidal currents. To quantify the spatial variability of contribution of each physical process in changing the momentum, the analysis is performed at three representative locations (Figure 1). Station A is to the south of Martha's Vineyard at approximately 30 m. Station B is chosen on Nantucket Shoals at the 20 m isobath, and finally station C is east of Cape Cod at the 30 m isobath. For both the u- and v- momentum equations, hourly time series of each term in the balance are plotted over a 24-hour window in Figure 24.

[30] At station A, we see a picture of term balances that is consistent with that identified by the abovementioned observational studies. In the u- (east-west/approximately along-isobath direction) momentum balance, the largest terms are local acceleration, pressure gradient and Coriolis. The latter two act in concert to balance the local acceleration. Bottom friction and advection are very small and their effects on the balance are negligible. In the v- (north-south/approximately across-isobath direction) momentum balance, the major balance is between local acceleration and Coriolis with pressure gradient largely balancing the residuals. Contributions from bottom friction and advection are again negligible; suggesting that the local tidal dynamics in the area are linear.

[31] Moving northeast to station B (Nantucket Shoals), we see a completely different dynamical picture; every term in the balance is significantly bigger (note the scale changes) than that at station A. Most strikingly, we see that bottom stress and advection has the same order of magnitude as the other terms. In the u- (east-west/approximately across-isobath direction) momentum balance, the largest two terms are the pressure gradient and advection, showing nonlinear dynamics becoming important. Notice that these two terms are periodic with the M_4 time period, indicating nonlinear generation of the shallow water tidal constituent (M_4 tide). This is not surprising, as complex island geometry and bathymetric irregularity of Nantucket Shoals, together with very strong tidal currents, can certainly give rise to strong nonlinearity in the system. The critical impact of the irregular bathymetry of Nantucket Shoals is also seen in the significantly enhanced bottom stress term, which is largely balanced by Coriolis. In the v-(north-south/approximately along-isobath direction) momentum balance, the pressure gradient remains as the largest term, and is mostly balanced by the sum of bottom stress, local acceleration, and advection. Notice here Coriolis is the smallest term in the balance, indicating the across-isobath velocity is small. This is consistent with the tidal current ellipses (Figure 15) showing the ellipticity of the M_2 tidal current is very weak on Nantucket Shoals, and thus the tidal current are largely in the along-isobath direction. All terms except advection are now periodic with the M_2 time period.

[32] Nonlinear advection and bottom stress become smaller at station C, where the bottom bathymetry becomes smooth again. The major balance in the u- (east-west/approximately across-isobath direction) momentum now is between Coriolis and pressure gradient. Tidal current in this area is still mainly in the along-isobath direction. As a result, Coriolis in the v-(north-east/approximately along-isobath direction) momentum remains small, and the balance is dominated by pressure gradient and local acceleration.

7. Summary and Conclusion

[33] A data assimilative modeling study of the barotropic tides on the New England Shelf is presented. This is

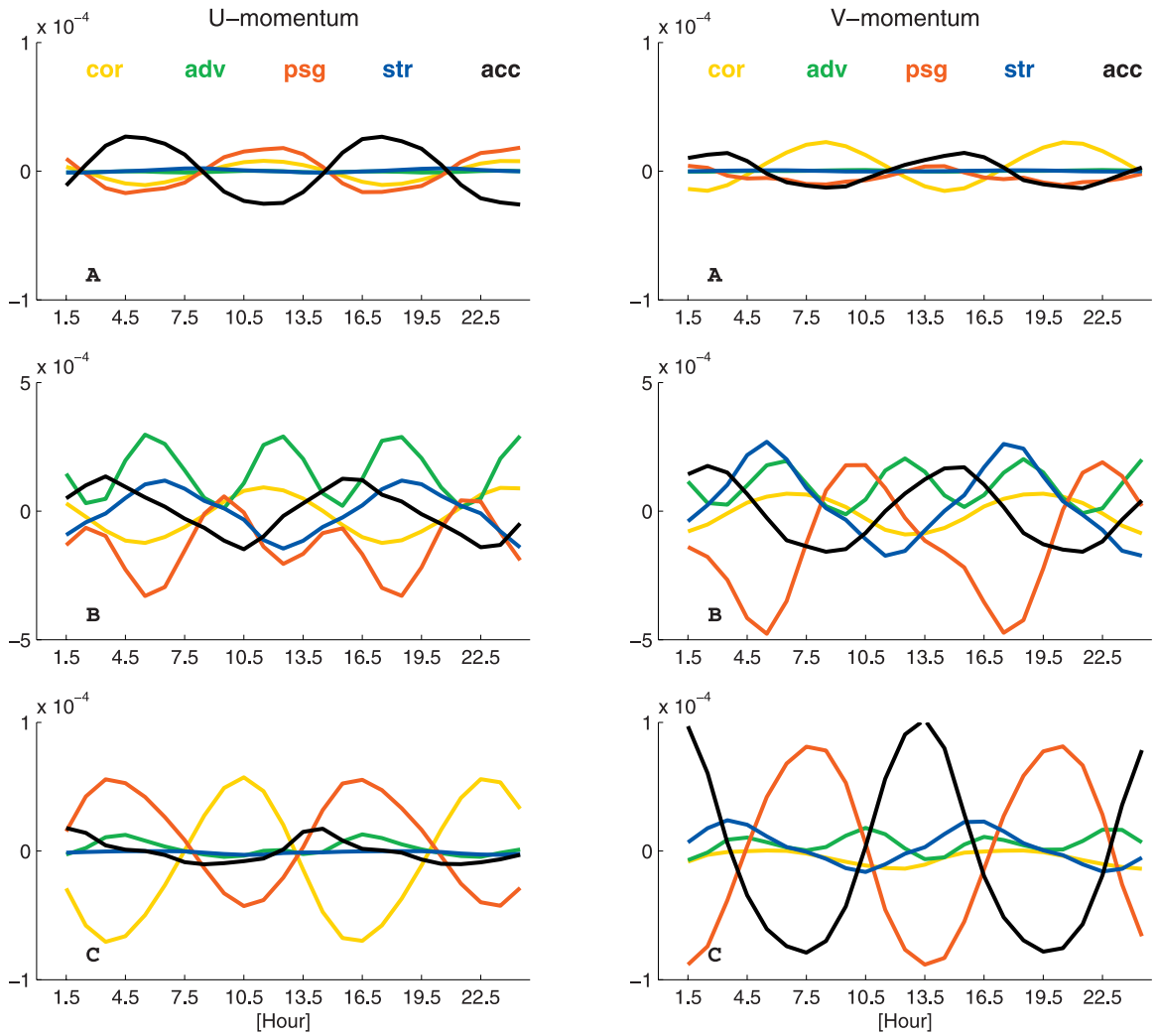

Figure 24. A comparison of depth-averaged momentum balance in the east (u) and north (v) directions for the M_2-series input from stations A, B, and C (Figure 1). The term unit is m s^{-2}. cor, adv, psg, str, and acc denote Coriolis term, advection term, pressure gradient term, bottom stress term, and local acceleration term, respectively.

motivated by a clear need to resolve the under-sampling problem pointed out by previous observational studies in the area [e.g., *Shearman and Lentz*, 2004] and aimed at improving our understanding of regional tidal characteristic and dynamics. We have focused on providing the best estimation of 5 major tidal constituents (M_2, S_2, N_2, O_1, and K_1). The first step to achieve this was to accurately specify OBCs for the regional model. Global/basin scale tidal models [*Shum et al.*, 1997; *Egbert et al.*, 1994; *Egbert and Erofeeva*, 2002; *Luettich et al.*, 1992] are commonly used to provide OBCs for regional coastal models. Although quite accurate in the open ocean, these large-scale models are often limited by their resolution of coastline details and coastal bathymetry, especially for a coastal region like New England Shelf which has many complex geometric and bathymetric features. As a result, significant tuning efforts are often required to adapt these global/basin-scale tidal solutions to achieve the accuracy demanded by a local tidal application.

[34] We devised a hybrid data assimilation modeling system consisting of a regional high-resolution ROMS as the forward model and TRUXTON as the inverse model. In situ tidal harmonics were assimilated via the incremental correction ("fine tune") for the prior barotropic tidal OBCs. Because ROMS and TRUXTON use different model grids and numerical schemes, care was taken to allow these two models work in tandem. Model skill was evaluated by comparing the misfits between the observed and modeled tidal harmonics. This hybrid data assimilation approach was found effective in correcting the tidal OBCs, which in turn improve ROMS tidal solutions. Up to 50% decreases of model/data misfits are achieved after inverse data assimilation. It should be noted that because TRUXTON is a frequency-domain model, it is highly efficient and fast in data inversion. Overall this hybrid data assimilation approach provides a better alternative to the otherwise empirical "trial-and-error" way to tune up regional tidal models. One caveat of our hybrid inverse approach is in the underlying assumption that model/data misfits are the solo

result of inaccurate specification of barotropic tidal OBCs. In reality, errors and uncertainties also arise from a variety of other sources, including errors in the observations themselves and model parameterizations such as bottom friction. With regard to the former, one needs to use accurate observations (and hence our decision to use pressures rather than current measurements in this study. Another reason for using pressure measurements is because of the pressure fields have larger scales than do the current fields; and thus are less subject to spatial aliasing of and internal tide contributions to current measurements). For the latter, more experiments may be needed in the future to explore model solution sensitivity to the frictional parameterization for which a more general inverse strategy is required. To that end, encouraging progress has now been made towards sensitivity analysis and generalized 4-dimensional variational data assimilation using tangent linear adjoint ROMS [*Moore et al.*, 2004] which in the future would allow the tidal data assimilation to be conducted entirely with the ROMS model.

[35] The ROMS tidal solutions were used to produce co-amplitude and co-phase maps for each of the 5 major diurnal and semidiurnal tidal constituents in this region. Significant variations in both tidal amplitudes and phases are identified, along with the unique tidal elevation minimum on Nantucket Shoals for all semi-diurnal constituents. In contrast, diurnal tides across the shelf are more spatially uniform. This is because the New England Shelf is between the dynamically distinct MAB shelf to the west and the (semi-diurnally) amplified GOM to the northeast. Semidiurnal tide elevations of these two regions are out of phase and counteract each other, resulting in relatively low tidal elevations in this transition zone. Overall, the tides on the New England Shelf can be characterized as mixed and mainly semi-diurnal type.

[36] Tidal current ellipse maps reveal that currents are strongest on Nantucket Shoals, which combined with rough and irregular bottom bathymetry, produce significant tidal mixing and energy dissipation. Momentum balance analyses on M_2 tides further confirm the complexity of tidal dynamics on the New England Shelf. Along-isobath pressure gradient is the dominant term across the entire shelf, while the contributions of other physical processes are spatially heterogeneous. This implies that unlike either of the region immediately to the west (MAB) or east (GOM), simple analytical models will not adequately reproduce tidal currents and elevations.

[37] **Acknowledgments.** This work was supported by WHOI Coastal Ocean Institute Research Award. R.H. thanks D. Lynch and K. Smith for providing TRUXTON model, helpful assistance in system design, and valuable discussions on coastal ocean modeling and data assimilation. J.W. acknowledges support of the Office of Naval Research. We thank K. Shearman, S. Lentz, and J. Trowbridge for providing tidal harmonics and CBLAST in situ measurements, and R. Luettich for supplying ADCIRC tidal harmonics database on-line. We are indebted to W. Geyer and R. Beardsley for their valuable insights and constructive reviews.

References

Aretxabaleta, A., J. P. Manning, F. E. Werner, K. W. Smith, B. O. Blanton, and D. R. Lynch (2005), Data assimilative hindcast on the southern flank of Georges Bank during May 1999: Frontal circulation and implication, *Cont. Shelf Res.*, *25*, 849–874.

Beardsley, R. C., D. C. Chapman, K. H. Brink, S. R. Ramp, and R. Schlitz (1985), The Nantucket Shoals Flux Experiment (NSFE79). Part I: A basic description of the current and temperature variability, *J. Phys. Oceanogr.*, *15*, 713–748.

Bothner, M. H., et al. (1981), Geochemical evidence for modern sediment accumulation on the continental shelf off southern New England, *J. Sediment. Petrol.*, *51*, 281–292.

Brown, W. S. (1984), A comparison of Georges Bank, Gulf of Maine, and New England shelf tidal dynamics, *J. Phys. Oceanogr.*, *14*, 145–167.

Brown, W. S., N. R. Pettigrew, and J. D. Irish (1985), The Nantucket Shoal Flux Experiment (NSFE79): II: The structure and variability of across-shelf pressure gradient, *J. Phys. Oceanogr.*, *15*, 749–771.

CCAT Research Program (2003), ADCIRC tidal databases. (Available at http://www.marine.unc.edu/C_CATS/tides/tides.htm)

Colosi, J. A., R. C. Beardsley, J. F. Lynch, G. Gawarkiewicz, C.-S. Chiu, and A. Scotti (2001), Observations of nonlinear internal waves on the outer New England continental shelf during the summer Shelfbreak Primer study, *J. Geophys. Res.*, *106*, 9587–9601.

Daifuku, P. R., and R. C. Beardsley (1983), The K_1 tide on the continental shelf from Nova Scotia to Cape Hatteras, *J. Phys. Oceanogr.*, *13*(1), 3–17.

Davies, A. M., S. C. M. Kwong, and R. A. Flather (1997), A three-dimensional model of diurnal and semidiurnal tides on the European shelf, *J. Geophys. Res.*, *102*, 8625–8656.

Defant, A. (1958), *Ebb and Flow: The Tides of the Earth, Air, and Water*, 122 pp., Univ. of Mich. Press, Ann Arbor, Mich.

Dickey, T. D., and A. J. Williams III (2001), Interdisciplinary ocean process studies on the New England shelf, *J. Geophys. Res.*, *106*, 9427–9434.

Divins, D. L., and D. Metzger (2003), NGDC coastal relief model, Natl. Geophys. Data Cent., Boulder, Colo. (Available at http://www.ngdc.noaa.gov/mgg/coastal/coastal.html)

Egbert, G. D., and S. Y. Erofeeva (2002), Efficient inverse modeling of barotropic ocean tides, *J. Atmos. Oceanic Technol.*, *19*(2), 183–204.

Egbert, G. D., A. F. Bennett, and M. G. G. Foreman (1994), TOPEX/POSEIDON tides estimated using a global inverse model, *J. Geophys. Res.*, *99*, 24,821–24,852.

Emery, W. J., and R. E. Thompson (2001), *Data Analysis Methods in Oceanography*, 658 pp., Elsevier, New York.

Flather, R. A. (1976), A tidal model of the northwest European continental shelf, *Mem. Soc. R. Sci. Leige, Ser. 6*, *10*, 141–164.

Foreman, M. G. (1977), Manual for tidal heights analysis and prediction, *Pac. Mar. Sci. Rep. 77-10*, Inst. of Ocean Sci., Victoria, B. C., Canada.

Greenberg, D. A. (1982), The contribution of modeling to understand the dynamics of the Bay of Fundy and Gulf of Maine, in *Modeling Marine System*, edited by A. Davies, chap. 5, pp. 108–138, CRS Press, Boca Raton, Fla.

He, R., D. J. McGillicuddy, D. R. Lynch, K. S. Smith, C. A. Stock, and J. P. Manning (2005), Data assimilative hindcast of the Gulf of Maine circulation, *J. Geophys. Res.*, *110*, C10011, doi:10.1029/2004JC002807.

Kowalik, Z., and A. Y. Proshutinsky (1993), Diurnal tides in the Arctic Ocean, *J. Geophys. Res.*, *98*, 16,449–16,469.

Limeburner, R., and R. C. Beardsley (1982), The seasonal hydrography and circulation over Nantucket Shoals, *J. Mar. Res.*, *40*, 371–406.

Luettich, R. A., J. J. Westerink, and N. W. Scheffner (1992), ADCIRC: An advanced three-dimensional circulation model for shelves, coasts and estuaries, U.S. Army Eng. Waterw. Exp. Stn..

Lynch, D. R., and C. E. Naimie (1993), The M_2 tide and its residual on the outer banks of the Gulf of Maine, *J. Phys. Oceanogr.*, *23*, 2222–2253.

Lynch, D. R., C. E. Naimie, and C. G. Hannah (1998), Hindcasting the Georges Bank circulation, Part I: Detiding, *Cont. Shelf Res.*, *18*, 607–639.

Lynch, D., K. Smith, B. Blanton, R. Luettich, and F. Werner (2004), Forecasting the coastal ocean: Resolution, tide, and operational data in the South Atlantic Bight, *J. Atmos. Oceanic Technol.*, *21*, 1074–1085.

Marchesiello, P., J. C. McWilliams, and A. F. Shchepetkin (2001), Open boundary conditions for long-term integration of regional oceanic models, *Ocean Model.*, *3*, 1–20.

Moody, J. A., et al. (1984), Atlas of tidal elevation and current observations on the northeast American continental shelf and slope, *U.S. Geol. Surv. Bull.*, *1161*, 1–122.

Moore, A. M., H. G. Arango, E. D. Lorenzo, B. D. Cornuelle, A. J. Miller, and D. J. Neilson (2004), A comprehensive ocean predication and analysis system based on the tangent linear and adjoint of a regional ocean model, *Ocean Model.*, *7*, 227–258.

Mukai, A. Y., J. J. Westerink, R. A. Luettich, and D. Mark (2002), Eastcoast 2001: A tidal constituent database for the western North Atlantic, Gulf of Mexico and Caribbean Sea, *Tech. Rep. ERDC/CHL TR-02-24*, 201 pp., U.S. Army Eng. Res. and Dev. Cent., Coastal and Hydraul. Lab., Vicksburg, Miss.

Munk, W. (1997), Once-again: Once again-tidal friction, *Prog. Oceanogr.*, *40*, 7–35.

NOS (2002), Harmonic tidal data. (Available at http://coops.nos.noaa.gov)
Pawalowicz, R., R. C. Beardsley, and S. Lentz (2002), Harmonic analysis including error estimates in MATLAB using T-TIDE, *Comput. Geosci.*, *28*, 929–937.
Shearman, R. K., and S. J. Lentz (2004), Observations of tidal variability on the New England shelf, *J. Geophys. Res.*, *109*, C06010, doi:10.1029/2003JC001972.
Shum, C.-K., et al. (1997), Accuracy assessment of recent ocean tide models, *J. Geophys. Res.*, *102*(C11), 25,173–25,194.
Simpson, J. H., and J. R. Hunter (1974), Fronts in the Irish Sea, *Nature*, *250*, 404–406.
Twichell, D. C., C. E. McClennen, and B. Butman (1981), Morphology and processes associated with the accumulation of the fine-grained sediment deposit on the southern New England shelf, *J. Sediment. Petrol.*, *51*, 266–280.
Zimmerman, J. T. F. (1978), Topographic generation of residual circulation by oscillatory (tidal) current, *Geophys. Astrophys. Fluid Dyn.*, *11*, 35–47.

R. He, Department of Applied Ocean Physics and Engineering, Woods Hole Oceanographic Institution, Mail Stop 12, Woods Hole, MA 02543, USA. (rhe@whoi.edu)
J. L. Wilkin, Institute of Marine and Coastal Sciences, Rutgers, The State University of New Jersey, New Brunswick, NJ 08901-8521, USA.